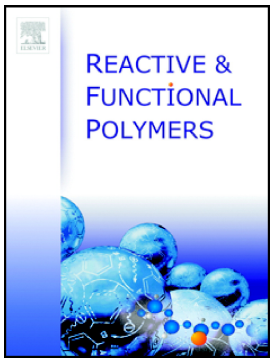
Accepted Manuscript



Influence of backbone structure, conversion and phenolic co-curing of cyanate esters on side relaxations, fracture toughness, flammability properties and water uptake and toughening with low molecular weight polyethersulphones

Christoph Uhlig, Monika Bauer, Jörg Bauer, Olaf Kahle, Ambrose C. Taylor, Anthony J. Kinloch

PII: S1381-5148(17)30200-6
DOI: doi:10.1016/j.reactfunctpolym.2017.10.004
Reference: REACT 3918

To appear in: *Reactive and Functional Polymers*

Received date: 22 December 2016
Revised date: 9 October 2017
Accepted date: 10 October 2017

Please cite this article as: Christoph Uhlig, Monika Bauer, Jörg Bauer, Olaf Kahle, Ambrose C. Taylor, Anthony J. Kinloch , Influence of backbone structure, conversion and phenolic co-curing of cyanate esters on side relaxations, fracture toughness, flammability properties and water uptake and toughening with low molecular weight polyethersulphones. The address for the corresponding author was captured as affiliation for all authors. Please check if appropriate. React(2017), doi:10.1016/j.reactfunctpolym.2017.10.004

This is a PDF file of an unedited manuscript that has been accepted for publication. As a service to our customers we are providing this early version of the manuscript. The manuscript will undergo copyediting, typesetting, and review of the resulting proof before it is published in its final form. Please note that during the production process errors may be discovered which could affect the content, and all legal disclaimers that apply to the journal pertain.

ACCEPTED MANUSCRIPT

Influence of backbone structure, conversion and phenolic co-curing of cyanate esters on side relaxations, fracture toughness, flammability properties and water uptake and toughening with low molecular weight polyethersulphones

Christoph Uhlig[a,*], Monika Bauer[a1], Jörg Bauer[b], Olaf Kahle[a], Ambrose C. Taylor[c], Anthony J. Kinloch[c]

[a] Fraunhofer Research Institution for Polymeric Materials and Composites PYCO, Kantstrasse 55, 14513 Teltow, Germany

[b] Fraunhofer Institute for Reliability and Microintegration IZM, Gustav-Meyer-Allee 25, 13355 Berlin, Germany

[c] Imperial College London, Department of Mechanical Engineering, South Kensington Campus, London SW7 2AZ, United Kingdom

* Christoph Uhlig, Christoph.uhlig@iap.fraunhofer.de, Tel +49 3328 330 290, Fax +49 3328 330 282

Abstract

The effect of backbone structure and conversion of polycyanurate networks on solid state properties has been studied and compared to co-curing with bisphenol-A. Dynamic mechanical behaviour, density, flammability properties, fracture toughness and long-term water uptake were investigated. The intensity of the γ-relaxation increases, room temperature density decreases with increasing conversion, both due to increasing free volume with increasing conversion. A brittle-ductile transition was detected by precise fracture toughness measurements; above a critical conversion the fracture toughness rises suddenly from extremely low values to a plateau or maximum: Networks with higher toughness show a maximum, those with lower toughness a plateau. Bisphenol-A modification causes intrinsic toughness variations. Toughening of two different cyanate esters with polyethersulphones synthesized with various molecular weights between 3000 and 10500 (M_n) was investigated. Significant

[1] Present Address: InnoMat GmbH, Kantstrasse 55, D-14513 Teltow, Germany, monika.bauer@innomat-gmbh.de

ACCEPTED MANUSCRIPT

toughening effects can be achieved already with intermediate molecular weights lower than those of commercially-available high-T_g amorphous thermoplastics. Long-term water uptake measurements at 28°C, 50°C and 70°C over two years show a non-Fickian part of the water uptake for all cyanate esters even at temperatures as low as 28°C. The effects of backbone structure, conversion and storage temperature are discussed in detail.

Keywords

cyanate ester; conversion; fracture toughness; water uptake; thermoplastic toughening

1 Introduction

Cyanate ester resins are high performance thermosetting polymers. In the cured state they are also called polycyanurates. A unique combination of properties such as high temperature stability, low moisture uptake and low dielectric constant in the cured state, plus low viscosity in the uncured state (lowest viscosity of all high temperature resins) has led to their use in low-volume high-performance applications [1]. In such applications, the use of these high-priced materials is justified by their excellent performance as well as a lack of alternatives. This lack of alternatives is one reason why their price remains high, and confines their application to a few low-volume applications such as space satellites, microelectronics, and radomes or airducts in aircraft.

Recently, the authors received requests from civil air and ground transportation companies to investigate the use of cyanate ester resins for higher-volume applications as composite parts in civil aircraft interiors and in motors at high temperature. There is also an increased interest in the use of new cyanate ester types in high-speed telecommunications. This move is driven by new trends: The number of cyanate ester resin producers has increased recently (and may increase even further), which may lead to reductions in price. Perhaps even more importantly, there is an increasing concern about health issues, mainly during production but also when thermoset materials are used in vehicles or aircraft. For instance, there are indications that the toxicity of phenolic resins might not be acceptable under future European regulations. There are also concerns about epoxy resins regarding allergic reactions to

ACCEPTED MANUSCRIPT

epoxy compounds, and the carcinogenicity of aromatic amine curing agents. New and stricter health and safety regulations will drive the search for less-toxic thermosetting resins. Cyanate esters seem to be the best existing alternative to both epoxy and phenolic resins. There are no concerns at all regarding toxicity of cyanates. Like epoxy resins they are addition-curing and exhibit comparable or superior thermal and mechanical properties, whereas for flammability properties they are far superior to epoxies and in the same range as phenolic resins.

Another driver for higher-volume use of cyanate esters is the need for high-throughput technologies for fibre composite production, such as high pressure resin transfer moulding (RTM). If properly formulated with co-monomers, cyanate ester resins combine the lowest viscosity of all resins possessing high glass transition temperatures (only vinyl ester resins or unsaturated polyester resins have lower viscosities) with an extremely high reactivity. There are also technologies available to combine latency and high reactivity [2]. All these factors justify the assumption that cyanate esters are ready to move from the specialty low-volume applications of the past to high-volume applications in the near future.

There are already a large number of publications on cyanate ester resins. These works were either motived by fundamental scientific considerations, since cyanate esters are an interesting model system for networks due to their uniform trifunctional network structure, or aspects which are relevant mainly in high-performance applications. However, aspects which are relevant in higher-volume applications have not been considered in sufficient detail, and this work addresses these gaps.

The maximum glass transition temperature (T_g) for the fully cured state (i.e. for maximum conversion, denoted T_g(max)) of nearly all commercially-available cyanate esters is much higher than that required in applications such as ground or air transport vehicles. The question is then: Do cyanate ester resins need to be fully cured for such applications? Further, phenolics, which are the current resins used for aircraft interiors, are not fully cured in most cases. If a conversion lower than the maximum is acceptable then the effect of conversion on the properties becomes highly relevant. This effect has been briefly reported in [3-7], but this work covers a broader range.

ACCEPTED MANUSCRIPT

Whereas in [3-7] the effect of conversion is investigated only for one cyanate ester monomer, two different cyanate ester monomers are compared here to show the effect of backbone structure. In the first part of this work high precision thermomechanical data (measured using a custom-built torsional pendulum) and precise measurements of conversion form the basis of an analysis over an extended range of conversion. A small part of these data has already been published in [8], but only in the context of analysing the formation of irregular structures in polycyanurate networks. The present work concentrates on networks from 2,2-bis(4-cyanatophenyl)propane (B10) and bis(4-cyanato-3,5-dimethyl)methane (M10) with regular structures, and an analysis of the influence of backbone structure and conversion on thermophysical properties is given.

This work also shows an interesting fracture phenomenon: a brittle-ductile transition which occurs within a narrow region of conversion and was not reported before. During the course of these investigations an improved technique to measure fracture toughness has been developed [9]. Using this new optical crack tracing (OCT) technique, this brittle-ductile transition has been investigated in more detail for five different cyanate ester resins. To the authors' knowledge there are no publications with such a broad range of high accuracy fracture toughness data for cyanate esters.

The fire-smoke-toxicity (FST) properties (i.e. flammability) of cyanate esters have been investigated using cone calorimetry [10-13], but the effect of conversion has not previously been studied. This work reports the effect of conversion on heat release rate as determined by cone calorimetry for four different cyanate ester resins.

The effect of the modification of cyanate esters with phenolics such as bisphenol-A on network structure comes closest to that of conversion [14-16]. The practical importance of phenolic modification lies in the fact that T_g(max) of the network (and thus the curing temperatures needed to achieve T_g(max)) can be dramatically reduced and the curing reaction is highly accelerated. However, no significant deterioration in flammability properties would be expected since the structural elements are nearly identical, and only the network density is reduced by phenolic modification. In this work the effects of modification of cyanate esters with bisphenol-A on both fracture and

ACCEPTED MANUSCRIPT

flammability properties have been studied and compared to the effect of conversion on these properties.

As will be shown, the fracture toughness of unmodified cyanate esters is relatively high in relation to their T_g. However, for their use as matrix resins for structural composites an increase in toughness would still be required. High-T_g amorphous thermoplastics (TPs) have been shown to toughen cyanate esters [17-36]. Commercial types of polysulphone or polyetherimide can be used, but due to the high molecular weight of all commercial TPs, this is at the expense of a large increase in viscosity of the cyanate-TP blend. Cyanate esters are especially suitable for manufacturing fibre composites using infusion processes such as vacuum infusion or resin transfer moulding (RTM) because of their low viscosity. Therefore it would be of practical interest if toughening can be achieved using lower molecular weight grades of such thermoplastics that do not increase the viscosity so much. For applications where low flammability is required, polyethersulphone (PES) seems to be the best choice as the toughening agent. There are a number of publications on polyethersulphone toughening of cyanate esters [17-36]. However, the present work investigates the low molar mass range of PES in more detail than any other study so far. Moreover, whereas other works have mainly concentrated on toughening of the bisphenol-A dicyanate, the present work compares polyethersulphone toughening for bisphenol-A dicyanate (B10) and a multifunctional novolac-type cyanate ester (PT-resin). As will be shown below, novolac-type cyanate esters are much more interesting for applications requiring low flammability. Furthermore, their toughness in the unmodified state is lower than that of bisphenol-A dicyanate, and therefore toughening of the PT-resins is of particular interest for many applications.

The sensitivity of polycyanurates to hydrolytic attack is well known [37]. Various aspects of moisture diffusion and degradation in water at elevated temperatures and at long times have been presented for pure and formulated cyanate ester resins [7, 38-47]. In some of these reports accelerated ageing conditions have been used. However, extrapolations from severe conditions of storage in water down to mild conditions cannot be made, since processes such as hydrolytic degradation are threshold processes which cannot be described by Arrhenius laws. Therefore, in the

ACCEPTED MANUSCRIPT

last part of the present work a detailed study on the long-term water uptake behaviour (up to 2.2 years) is presented for five different cyanates with different conversions. The effect of conversion and backbone structure on Fickian and non-Fickian water uptake is discussed. To investigate the realistic long-term behaviour in the typical range of operating temperatures, 28°C, 50°C and 70°C were chosen as the isothermal water bath temperatures.

2 Experimental

2.1 Materials

The cyanate ester resins used are listed in Table 1 together with their chemical structures, trade names, producers and alternative designations in literature. In this work the former trade names of Rhone-Poulenc (now Huntsman USA) are used for the di-functional cyanate esters. For the cyanate ester resins of higher functionality the respective trade names of DOW and Lonza are used. For a better understanding abbreviations referring to structure are used additionally in case of two monomers (B10 (DCBA) and M10 (TMDCBF)). Bisphenol-A (BA) used as co-monomer for cyanate esters was obtained from Sigma Aldrich (purity >99%).

For the synthesis of linear bisphenol-A polyethersulphone (PES) different batches of 4,4'-dichloro-diphenylsulphone (CPS) were obtained from Aldrich and Fluka, and of bisphenol-A (BA) from Merck, with varying purities between >96% and >98%. Purity was controlled by melting point (via hot stage polarized microscope) and thin layer chromatography (mobile phase hexane/acidic ester/methanol 6:3:1). To achieve high molar masses in the synthesis, in some cases the CPS and BA were purified by recrystallization using toluene. When this purification was performed the purity was controlled by HPLC, in all other cases the purity data from the producer were used. The CPS and BA were reacted in a molar ratio of 1:1 (taking into account purity information either from HPLC or the producer). The synthesis was carried out following Scheme 1.

Example of a synthesis of a linear bisphenol-A polyethersulphone:
In a 500 ml three necked flask equipped with an N_2-inlet, thermometer, reflux condenser and magnetic stirrer, 25.0 g (98.33 mmol) 4,4-dichloro-diphenylsulphone

ACCEPTED MANUSCRIPT

(CPS) were dissolved in 100 ml dimethylsulphoxide at 50°C. To this solution 22.67 g (99.31 mmol) bisphenol-A (BA) was added dissolved in 50 ml dimethylsulphoxide. After all components were dissolved, 27.55 g (198.57 mmol) K_2CO_3 in 100 ml dimethylsulphoxide were added to the reaction mixture. The mixture was stirred at 165°C for 10 h. During the course of synthesis the decrease of monomers was qualitatively monitored by thin layer chromatography. The crude reaction product was precipitated in 500 ml water / 50 ml HCl and then washed with water and dried on a rotary evaporator. It was then dissolved in tetrahydrofuran (THF) and precipitated in water/isopropanol (1:1). The resulting product was again dried on a rotary evaporator. In the next purification step the product was dissolved in THF/CH_2Cl_2 (2:1) and again precipitated, this time in ethanol. The product was dried on a rotary evaporator until its weight remained constant. Size-exclusion chromatography (SEC) was performed in THF on all synthesized batches. To determine molar masses, an UV detector and polystyrene calibration was used.

By synthesizing PES either using purified or as-received monomers a range of molar masses between M_n = 3720 and M_n = 11720 was obtained, this range was a result of the different purities of the different batches of monomers used (lower molar masses) and of purification (higher molar masses).

To produce bulk polymer plates, the cyanate esters (or mixtures of cyanate esters with bisphenol-A) were melted and degassed (at 130°C for M10, at 90°C for all other types). The molten resin was poured into pre-heated vertical aluminium alloy moulds (160 mm x 100 mm x 6 mm), treated with mould-release agents. The cast plates were cured using programmable forced-air circulating ovens. Temperature profiles of the curing cycles were recorded using a temperature sensor within the oven near the moulds.

More than 50 different curing cycles were used to reach as many different conversions as possible. This was done partly by a trial and error approach, but mainly driven by the need to cure as many castings in one curing cycle as possible, thereby combining cyanate esters with different reactivity. The lowest curing temperature used was 120°C; the highest curing temperature was 300°C. For higher curing temperatures isothermal steps (typically every 20 to 40°C depending on reactivity) at lower

ACCEPTED MANUSCRIPT

temperatures were programmed to avoid exothermic effects. The ramp rate used between the isothermal steps was 1°C/min. Since curing cycles have been chosen to obtain as many different conversions as possible and no relationships between curing cycles and properties are discussed here, the detailed curing cycles used are not relevant and therefore are given only when where the conversion (or measure of conversion) has not been measured.

Conversion was measured (see Section 3.1 and 3.4) using a combined procedure of size-exclusion chromatography (SEC) and Fourier-transform infrared spectroscopy (FTIR), as described in detail in [48]. An alternative approach to determine a measure of conversion (as used in Section 3.2 and 3.3) is described in detail in Section 3.2.

Synthesized and commercial polyethersulphones were used. These were dissolved and mixed with PT15 and B10 in methylene chloride. The solvent was thoroughly removed in a rotary evaporator before the mixtures were poured into the moulds and cured as described above.

All specimens were machined from the same cast plate (with the exception of cone calorimetry samples, where extra castings were produced in some cases). Rods of 100 mm x 10 mm x 3 mm were machined for torsional pendulum tests. Rods of 44 mm x 6 mm x 3 mm were used for dynamic mechanical analysis (DMA). Three compact tension (CT) specimens, where W = 35 mm according to [49], were used for fracture toughness measurements. These were machined using a diamond saw and a CNC milling machine. Samples for water uptake measurements of 30 mm x 20 mm, with a thickness varying between 1.5 mm and 2 mm, were machined using a CNC milling machine. For cone calorimetry specimens of size 60 mm x 60 mm x 6 mm were cut using a diamond saw.

2.2 Methods

Torsional pendulum (high-precision DMA): A custom-built torsional pendulum was used for high-precision dynamical mechanical analysis (DMA) in Section 3.1. The measurements used a temperature ramp rate of 2°C/min starting from -189°C. The

ACCEPTED MANUSCRIPT

frequency was kept constant at 1 Hz by manually changing the rotating discs during measurement.

DMA: A commercial dynamical mechanical analyser (Torsion Head-Mark II, Polymer Laboratories) was used for DMA measurements in Sections 3.2-3.4. Measurements were performed at a temperature ramp rate of 4°C/min and a frequency of 1 Hz.

TEM: A LEO 912 (Zeiss) was used for transmission electron microscopy (TEM). Thin sections were microtomed using an Ultra-Mictrotom (Leica), and were used without further staining in the transmission electron microscope.

Density: Density was measured on samples of 10 mm x 10 mm x 6 mm using a Helium pycnometer (Pycnomatic ATC, Porotec).

Fracture toughness: Fracture toughness (critical stress intensity factor, K_{Ic}) in Section 3.1 was measured in the classical way following the Standard [49] closely. Over the course of this work an improved method to measure the fracture toughness was developed called optical crack tracing (OCT) [9]: The crack length *a* is measured during the fracture test on the same time basis *t* as used for measuring load *P*. From the measured *P(t)* and *a(t)* data, the stress intensity factor can be calculated as a function of crack length $K_I(a)$ (called the "elastic R-curve"), the critical stress intensity factor $K_{Ic}(a)$ is taken the plateau of the $K_I(a)$-curve. The fracture energy $G_{Ic}(a)$ can be calculated using the area method from the same data. The measured data and fracture mechanics analysis are shown schematically in Fig. 1. A significant advantage of this method is that it eliminates artefacts caused by imperfect pre-cracks. Twisted pre-cracks, or pre-cracks with steps, cause mode II contributions to the fracture toughness, and thus significantly increase the measured value. This is likely to be why fracture toughness data in literature are often too high. This main error source for fracture toughness measurements (when using the Standard procedure) is highest for brittle specimens (in the range of K_{Ic} from 0.1 to 0.7 MN*m$^{-3/2}$). Such errors can be eliminated by measuring the R-curve using the OCT technique: During crack propagation the crack path follows the path of least energy, which is in mode I fracture. Therefore, in the plateau region of the R-curve the same value is always measured by

ACCEPTED MANUSCRIPT

OCT, as seen in Fig. 2. Fracture toughness can be measured to a very high accuracy using the OCT technique, especially for brittle specimens. Three CT-specimens (W = 35 mm) were machined from each casting and tested at a crosshead speed of 1 mm/min.

Viscosity: Dynamic (complex) viscosity was measured using a strain-controlled rheometer (ARES, Rheometrics) at 3°C/min and 1 Hz, with a plate-plate geometry (25 mm diameter).

Cone Calorimetry: A cone calorimeter (Fire Testing Technology) was used to measure the heat release rate according to ISO 5660. A cone-shaped infrared radiator was used to irradiate the specimen surface at a defined heat flux of 50 kW/m². This heat flux has been found to be suitable for testing interiors of aircraft and railway vehicles. Data were collected every one to five seconds to allow continuous monitoring of the combustion process. The time to ignition and the duration of the combustion process were recorded. The concentrations of oxygen, carbon monoxide and carbon dioxide were monitored to calculate the heat release rate. The determination of the heat release rate is based on the oxygen consumption principle: The effective heat of combustion of a large variety of commonly-used organic materials is about 13.1 MJ per kilogram of oxygen consumed. The smoke formation was also measured, but not shown here. The mass of the specimen was monitored continuously during the combustion process.

Water Uptake: The gravimetric water uptake samples, 20 mm by 30 mm in dimensions, were cut from sheets typically 1.5 mm to 2.0 mm thick. The samples were dried by placing them in an oven at 70°C, removed at intervals and weighed. All the sample weights were recorded to ± 0.1 mg, and when no further weight loss was measured over a period of at least 48 hours, they were assumed to be dry.
The samples were weighed before the water diffusion tests commenced. Their thickness was also measured, to ± 0.01 mm, using a micrometer. The samples were placed individually in small glass jars filled with distilled water, and placed in a water bath at the required temperature. Immersion temperatures of 28, 50 and 70°C were used. The samples were removed and weighed at intervals, of 15 minutes initially, but

ACCEPTED MANUSCRIPT

the time interval between measurements was increased as the rate of water uptake decreased. The total exposure times vary from sample to sample, as the samples were manufactured in several batches, and the samples thicknesses also vary. Hence all data are quoted at equal values of $t^{1/2}/l$, where t is the exposure time and l is the sample thickness.

List of Symbols

γ-relaxation	(Small) transition in polymer typically at around -100°C
a	Crack length (in fracture toughness test) [mm]
G'	Storage shear modulus [Pa, MPa]
G''	Loss modulus [Pa, MPa]
G_{Ic}	Critical strain energy release rate (fracture energy) [N/m]
HRR	Heat release rate [kW/m²]
K_{Ic}	Critical stress intensity factor (fracture toughness) [MN/m$^{3/2}$]
l	Thickness of sample [mm]
M_n	Number average molecular weight [g/mol]
M_w	Weight average molecular weight [g/mol]
P	Load [N]
t	Time [s, h]
$t^{1/2}/l$	Square root of time normalized by sample thickness [s$^{1/2}$/mm]
tan δ	Loss factor, tan δ = G''/G'
T_g	Glass transition temperature (defined at maximum of tan δ curve) [°C]
THR	Total heat release [MJ/m²]

3 Results and Discussion

3.1 Effect of conversion on thermomechanical and fracture properties – comparison of B10 (DCBA) and M10 (TMDCBF) cyanate esters

The storage modulus G' and the loss factor tan δ measured using the torsional pendulum are shown in Figs. 3 and 4 for networks of B10 and M10 cured to different conversions respectively. The glass transition temperatures were determined from the tan δ curves (T_g is defined at the peak of tan δ unless otherwise stated). The relationship between T_g and conversion is shown in Fig. 5, where a linear fit gives a good representation of the data within the investigated range of conversion, which

ACCEPTED MANUSCRIPT

justifies the approach to take T_g as a measure of conversion, as explained in detail in Section 3.2. There are some deviations for B10 at high conversions, which can be explained by a broadening of the tan δ peak caused by post-curing during the DMA measurement, which is discussed further in Section 3.2. In addition, the value of T_g(max) varies within 10 to 20°C for B10 depending on the reaction path (i.e. on the detailed curing cycle), which is not yet clearly understood. Conversion is directly related to the crosslink density, so the different gradients for B10 and M10 (with a steeper slope but lower T_g at the same conversion for M10) clearly demonstrate the influence of backbone structure on T_g and thermophysical properties in general, which will be discussed further below.

The density at room temperature for B10 and M10 as a function of conversion is compared in Fig. 6. Again, the points for B10 and M10 fall on different lines with different slopes; the density of B10 is less dependent on conversion than for M10. It is generally accepted in the literature that the influence of conversion on density is caused by the frozen-in free volume: The higher the conversion then the higher the value of T_g and consequently the higher the frozen-in free volume, resulting in a lower density [3,7]. The fact that the density of M10 is more dependent on conversion than that of B10 can be explained by a higher free volume frozen in for M10 due to the methyl groups in the ortho position.

In Fig. 7, the storage modulus G' (from torsional pendulum measurements) at room temperature (RT) is plotted versus the density. As expected there is a linear relationship between the density and storage modulus, and the points fall on different lines with different slopes for B10 and M10 again.

Whereas the effects of conversion on free volume have been discussed in the literature [3,7], the relationship between free volume and side relaxations has not been considered so far. Georjon and Galy [7] discuss the influence of conversion on volume-related properties, and the influence of conversion on side relaxations is discussed for B10 (DCBA) in [5,6]. The authors discuss the relationship between the room temperature modulus and the intensity of low temperature side relaxations (denoted as γ-relaxation). They propose that the dependence of storage modulus on conversion is a consequence of the intensity of the γ-relaxation. This is certainly the case if the modulus below the γ-relaxation is independent of conversion. In Fig. 8 the value of log(tan δ) at the maximum of the γ-relaxation is plotted as a function of

ACCEPTED MANUSCRIPT

conversion for B10 and M10. The points for B10 and M10 nearly fall on the same line, but this is an artefact since it is the area under the peak which represents the intensity of the relaxation, not the peak height. It can be seen in Figs. 3 and 4 that this area is generally larger for the γ-relaxation of B10, since the peak is broader for B10. The peak area of the tan δ peak is difficult to determine, but an alternative representation is given in Fig. 9, where the storage modulus as a function of conversion at -189°C (i.e. at a temperature below the γ-relaxation) and at room temperature are compared for B10 and M10. It is seen that the relaxation strength of the γ-relaxation which can be defined as the difference between the unrelaxed and relaxed modulus values [50] (defined as $\Delta G' = G'(-189°C) - G'(RT)$) is higher for B10 than for M10, corresponding to the generally larger area under the tan δ peak for B10.

It is often attempted to assign a set of molecular motions of well-defined chemical structural elements of the network to γ-relaxations (e.g. [6]). However, it may be argued that concentration of structural elements and how they are connected with each other in polycyanurate networks change with conversion. If there was a clear relationship between a defined set of molecular structural elements and the γ-relaxation then a change of shape and peak temperature of the γ-relaxation would be expected if the concentration of these groups varies, i.e. if conversion is varied. However, only the intensity of the γ-relaxation changes with conversion, but there are no significant changes in the peak shape or peak maximum temperature. This clearly highlights the dominance of free volume on the γ-relaxations over that of the chemical nature of structural elements and their respective concentration in the network, at least in the case of polycyanurate networks.

It can be seen in Fig. 7 that there is a good proportionality between the storage modulus and density at RT. It might be reasonably argued that there should also be a proportionality between G' and density at -189°C. Now, it is seen in Fig. 9 that the relaxation strength of the γ-relaxation of M10 is lower than that for B10, so it can be concluded that packing (i.e. the reduction of free volume) is still hindered by the bulkier backbone structure of the M10 (methyl groups in ortho-position) when cooling down through the γ-relaxation, i.e. the M10 network is less densely packed than the B10 network even at temperatures below the γ-relaxation. Interestingly, not only is the magnitude of the relaxation strength (as seen in G'(-189°C) - G'(25°C) higher for B10

ACCEPTED MANUSCRIPT

than for M10, but also its dependence on conversion is higher, as seen in Fig. 9. As there is less ability for close packing when cooling down through the γ-relaxation for the M10 polycyanurate networks, then also a lower influence of conversion on the degree of packing can be expected.

Fracture toughness

The fracture toughness (critical stress intensity factor K_{Ic}) is shown in Fig. 10 for the B10 and M10 polycyanurates. These data were measured using the classical procedure from the Standard [49], therefore there is some uncertainty involved as explained in Section 2.2 above. As will be shown in Section 3.2, these data could be reproduced largely using the more accurate OCT measurement technique.

The fracture toughness decreases with conversion, and there seems to be a brittle to ductile transition which is controlled by conversion. Below a critical conversion the material is a hard solid and extremely brittle, so that it was impossible to measure fracture toughness at this stage because the material broke already when CT-specimens were machined from the plates. Fracture toughness data below this transition (i.e. in the "brittle" state) were measured using an improved technique (see below). However, the importance of the data in Fig. 10 lies in the accurate determination of conversion, and thus a localisation of the brittle-ductile transition on an absolute conversion scale. Since fracture toughness in the brittle state could not be measured at this stage, the conversion for this brittle-ductile transition was derived from the brittle behaviour of specimens below this transition. This is marked by arrows in Fig. 10.

It is interesting to note that when fracture data are plotted versus conversion, the brittle-ductile transition appears at different conversions, whereas in the plot of the same data versus T_g (Fig. 11) the points for B10 and M10 fall nearly on a single curve. Thus the ductile-brittle-transition occurs at the same T_g rather than at the same conversion. To the authors' knowledge this phenomenon has not been described in the literature. It is not yet well understood, but there are indications that it might be a general phenomenon of all high-T_g thermosets. At low conversions there is a high sol content and the intermolecular connectivity of the network is low, interrupted by a rather high content of oligomeric branched molecules loosely connected or not connected at all to the network. The connectivity of the network is too low to sustain

ACCEPTED MANUSCRIPT

the stress concentration at the crack tip. The transition appears to be rather sharp. Further work is needed to explain this phenomenon and to understand the structural parameters controlling this transition.

3.2 Fracture and Flammability Properties for XU366, B10, L10, PT-resins and modifications of these with bisphenol-A

T_g derived from tan δ curves (i.e. from DMA) as a measure of conversion

It was shown above that the plot of T_g determined from DMA tanδ curves versus conversion determined by FTIR/SEC can be well represented by a linear fit in the investigated range of conversion. This means that T_g determined using DMA can be taken as a measure of conversion. Such DMA curves for XU366, L10, B10, PT15 and PT30 cured to different conversions are shown in Figs. 12 to 16 (only a selection of all the curves measured is shown).

The T_g was determined from the tan δ curves as follows: When there was a distinct tan δ peak which was not significantly broader than the peak for the polycyanurate with maximum conversion, then the peak temperature was taken as T_g. However, the tan δ peak can broaden because further curing shifts the peak to higher temperatures during DMA, and this overlay of peaks results in a broadened peak with no clear maximum. In such cases T_g was determined by fitting a "standard peak" to the low temperature flank of the tan δ peak as shown schematically in Fig. 14.

The disadvantage of taking this DMA-T_g as a measure of conversion is that it is proportional to conversion, but is not a conversion in absolute units such as that determined from FTIR or DSC. The advantage is that accuracy does not depend on conversion, whereas at high conversions (between 90 and 100%) both DSC and FTIR determinations become much less accurate. A second advantage lies in the high reproducibility of the DMA curves, especially the tan δ curve. If two neighbouring pieces are cut out from the same casting and measured by DMA then the tan δ curves generally fall nearly onto the same curve. The FTIR/GPC procedure of [48] can reach the same level of accuracy/reproducibility in the conversion range between 0% and 90%, but a significantly higher experimental effort is involved. For more technical types of cyanate esters such as PT15 and PT30 (which contain not just one pure monomer but a distribution of oligomeric units) as well as for combinations of cyanate esters with

ACCEPTED MANUSCRIPT

bisphenol-A the determination of conversion by the FTIR- and SEC-procedure given in [48] is more complicated to perform than for very pure cyanate esters such as B10 and M10, and at the same time is less accurate. Finally, using T_g from DMA as a measure of conversion is a very efficient way to analyse a large number of castings.
In [6] a DSC procedure was used to determine conversion for castings, i.e. for samples cured outside the DSC pan, but no details were given about how this was done. In the experience of the authors it is impossible to obtain reproducible results of conversion and T_g for cured resin specimens that have been cured outside the DSC pan. Therefore it is supposed that in [6] an extra sample of resin in a DSC pan was cured in the oven in parallel with the castings. However, in the experience of the authors there can be large differences in conversion between a large (>100 g) casting and the 0.02 g of resin in the DSC pan, even when cured in parallel. This is very likely to be due to autocatalytic effects. Therefore determination of conversion by DSC is not practical and accurate. Further, assessing the state of cure by DMA has a very practical meaning, as it is the only method that works for both neat resin castings and for composites.

Fracture properties

The fracture toughness of five different cyanate ester resins is shown in Fig. 17. These data were measured to a higher accuracy than the data in Figs. 10 and 11 using the new OCT technique (see Section 2.2). Along with a much-improved technique to mill out specimens using a CNC milling machine it was possible to measure fracture toughness data below the brittle-ductile transition, i.e. in the brittle range, so these results confirm the existence of this brittle-ductile transition with a sufficiently high number of consistent results. It is interesting to note that the T_g (as a measure of conversion) for the brittle-ductile transition is not the same for all of the cyanate esters investigated, and is in the order: PT30 ~ PT15 < L10 < XU366 < B10. This further substantiates the explanation given above that there is a critical connectivity at which the transition from brittleness to ductility takes place. It is reasonable that this connectivity is reached at a lower T_g for multifunctional resins (PT30, PT15) than for di-functional resins. The fact that the transition occurs at a higher T_g for XU366 than for L10 (although T_g(max) is much lower for XU366 than for L10) can be explained by similar arguments. As the molecular weight of the XU366 backbone structure is higher

ACCEPTED MANUSCRIPT

than that of L10 (three aromatic rings in XU366, versus two in L10), then the critical connectivity is reached at a higher T_g for XU366. However, B10 falls outside of this ranking, since it has a backbone structure which is similar to that of L10, but the transition occurs at a much higher T_g for B10 than for L10. This might be explained by the fact that B10 has a very strong tendency to crystallize, unlike XU366, L10, PT15 and PT30. At the brittle-ductile transition seen in Fig. 10, at about 72% conversion, there is still a significant proportion of unreacted monomer [48]. The tendency of these residual monomers to crystallize, perhaps combined with a tendency of the bisphenol-A type backbone structure containing low molecular weight oligomers (trimers, pentamers, etc.) to establish a crystalline order (or at least some kind of order), might contribute to the embrittlement (in addition to the connectivity argument), thereby shifting the brittle-ductile transition to higher conversions and thus higher values of T_g. However, this is still speculative, and more work is needed to fully understand this phenomenon.

This is not just a fundamental science consideration, but may have practical importance. In many applications there is a step between cure and post-cure where parts are moved, and thus they are subjected to mechanical forces before they are fully cured. In such cases it may be necessary to cure parts to a state above the brittle-ductile transition before handling them to prevent internal damage or cracks because of the very low fracture toughness in the brittle region (K_{Ic} in the range of 0.1 and 0.2 $MN*m^{-3/2}$, or even lower).

The second interesting feature in Fig. 17 is that the increase of fracture toughness with decrease of conversion (in the “ductile” region) is very different for the investigated cyanate esters. It scales with the fracture toughness in the fully cured state: The higher the value of K_{Ic}(max.conversion), the greater the increase in K_{Ic} when lowering the conversion. PT30 has the lowest fracture toughness and does not show any increase in K_{Ic} with decreased conversion, while PT15 shows only a very small increase. In rubber toughening it is well known that the toughening effect is controlled by the ductility of the matrix: the higher the ductility of the matrix, the higher is the toughening effect induced by the rubber particles. Reducing the network density by reducing conversion may act in a similar manner to rubber particles (local fluctuations in crosslink density which might lead to local “soft spots”) then the explanation of the influence of ductility on “toughenability by reducing network density” could be along the

ACCEPTED MANUSCRIPT

same line of argument. However, there might be an alternative explanation: In the experience of the authors while investigating fracture toughness of many different thermosets (EP-, UP-, VE-, PU- and silicone resins [51]) a correlation was generally seen between the shape of the tan δ peak and fracture toughness. Analysis of the data is complicated since other factors influence fracture toughness and this matter is not yet fully understood, but nevertheless the correlation seems significant and universal: Narrow, symmetric (and thus high) tan δ peaks correlate with high fracture toughness, broad, asymmetric (generally exhibiting a shoulder on the low temperature side) and thus lower tan δ peaks correlate with low fracture toughness. The data in the present work confirm this correlation. The tan δ peaks are broad, asymmetric and low for PT30 (and to a lesser extent also for PT15), see Figs. 15 and 16. And they are narrow, symmetric and high for B10, L10 and XU366; see Figs. 12 to 14.
There also appears to be a correlation between shape of the tan δ peak and the post-yield behaviour in compression in different classes of resins. Narrow, symmetric and thus high tan δ peaks correlate with strain softening after yield, whereas broad, asymmetric and thus low tan δ peaks lead to strain hardening in the post-yield region. This leads to the hypothesis that a uniform network (as indicated by a narrow, symmetric and thus high tan δ peak) is capable of absorbing a greater amount of energy than a non-uniform network, or in more physical terms, that it is not just the yield point but also (or even more significantly) the post-yield behaviour which controls fracture toughness and toughenability.

Fracture toughness data are shown in Fig. 18 for B10 modified with 5, 10, 15 and 20 wt-% of bisphenol-A (BA). It is important here to repeat the statement of the Section 2.2 above: The OCT technique, used to measure fracture toughness is very accurate, experimental errors are in the range of the size of the symbols in Fig. 17. Because of this high accuracy and reliability of OCT it can be established beyond doubt that the error bars given in Figs. 18 and 19 represent an intrinsic variation of fracture toughness, i.e. within one casting there are regions (with a size likely to be in the order of hundreds of microns at least or even in the range of millimetres) which vary in fracture toughness. The size of the error bars represent the difference between the lowest and highest fracture toughness value measured within one casting. At a fracture toughness higher than about 0.7 $MN*m^{-3/2}$ (K_{Ic}) crack propagation behaviour

ACCEPTED MANUSCRIPT

generally changes from continuous to stick-slip for all polycyanurate networks investigated in this work. The intrinsic variation of fracture toughness in BA-modified cyanate esters manifests itself not only in variations between the three CT-specimens machined out of one casting but also within the R-curves measured for one CT-specimen. There are stick-slip lines with largely varying fracture toughness values (for crack initiation, i.e. the tip of stick-slip line) within one measurement, i.e. one R-curve, whereas in macroscopically uniform materials exhibiting stick-slip behaviour (such as rubber toughened thermosets) the variation in initiation fracture toughness between the stick-slip lines of the R-curve is typically quite low (< 2%). Thus, there is no doubt that these large variations of fracture toughness are intrinsic. The effect of modification of cyanate esters with BA is also an increase in fracture toughness (not surprising, because BA decreases network density), but it is important to state that the effect of BA-modification is much more the intrinsic fracture toughness variation than the increase of the mean values.
Also the BA-modified B10 polycyanurates exhibit a brittle-ductile transition, as seen in Fig. 18, which gives further support to the assumption that this is a general phenomenon for all high T_g resins.

In Fig. 19, fracture toughness data are shown as a function of conversion (represented by T_g) for four types of cyanate esters modified with BA: B10 (same data as Fig. 18), XU366, PT15 and PT30. Fewer modifications were investigated for XU366 and the PT-resins compared with B10, therefore no distinction between the contents of BA (ranging from 5 to 20%) is made in Fig. 19. Also, there seems to be no clear influence of the BA content on the magnitude of intrinsic toughness variation. However, it can be seen that the effect of BA on the intrinsic variation of fracture toughness scales again with the fracture toughness of the neat and fully cured cyanate ester: Intrinsic variation is highest for BA-modified XU366, still very high for BA-modified B10, low for BA-modified PT15 and the lowest (hardly seen) for BA-modified PT30. This confirms that the effect of BA-modification is an increase in the intrinsic variation of fracture toughness rather than in the mean value: There is only a small intrinsic variation of fracture toughness for the PT-resins, but there is also no significant increase in the fracture toughness for these networks. The opposite is true for XU366 and B10. Thus (apart from the special effect of intrinsic variation) the effect of BA on fracture

ACCEPTED MANUSCRIPT

toughness is similar to that of conversion. This confirms that the effect of BA and phenolics in general on network-topological parameters is similar to the effect of conversion [14-16]. It is therefore reasonable to assume that models to explain both influences would be similar (again except for the effect of local fluctuations in BA-modified networks), as already outlined above for the effect of conversion.
It can only be speculated about the reasons for this intrinsic variation of fracture toughness: The reactivity of phenolics (such as BA) with cyanate esters (or actually with the triazine ring) is much higher than the reactivity of the 100% pure cyanate esters. Additionally the BA molecule is more polar than the cyanate ester monomer (or rather is the phenolic group more polar than the OCN-group, and much more polar than the triazine ring). These factors (either together or alone) might lead to macroscopic regions of different crosslink density and thus different fracture toughness. Again, further work is needed to substantiate this argument.

Flammability Properties

Heat release rate (HRR) curves of several B10 castings cured using the same curing cycle (280°C maximum curing temperature) are shown in Fig. 20. The corresponding total heat release (THR) curves, the integral of the HRR data, are shown in Fig. 21. It can be seen that there are variations which increase at longer times. Although cone calorimetry is the most advanced characterisation tool for fire-smoke-toxicity (FST) behaviour, some variations in measuring the heat release are inevitable. This is due to the complexity of material behaviour when burning, especially at the later stages of fire. For instance, cracks form during fire which create new surfaces for the fire, and such fracture behaviour is always stochastic to some extent. This variation of curves has to be kept in mind when discussing the influence of material variables such as conversion on heat release rate. In all cases an error envelope has to be assumed about the size of that shown in Fig. 21.
In Figs. 22 to 26 the THR is shown for five different cyanate ester resins (XU366, L10, B10, PT15 and PT30) cured to different degrees of conversion (T_g is taken as a measure of conversion). THR curves are shown because they are easier to compare than HRR curves. Only one curve for each curing state has been measured. The general trend is that with higher conversions (i.e. higher T_g) the THR reduces and shifts to longer times (i.e. ignition and development of fire is postponed), even

ACCEPTED MANUSCRIPT

considering the typical variations as shown in Fig. 21. Such behaviour is expected because the crosslink density is increased, and because higher curing temperatures were used to achieve higher conversions. These higher temperatures lead to the evaporation of volatile components and the beginning of oxidation of structural elements (such as methyl groups), all of which will reduce the concentration of volatile and readily-flammable components. Equally, the sol content decreases with increasing conversion [48].

When THR curves for similar T_g (as a measure of conversion) are compared the following ranking can be established: XU366 > B10 > L10 > PT15 > PT30. This can be explained by the respective chemical structure of the network: THR is lower when the N-content (from triazine ring) is higher, and it is higher when the content of methyl groups is higher. The structure of the backbone also has an influence, as the novolac structure gives a lower heat release rate than a backbone structure such as that from bisphenol-A. Thus the PT-resins have much lower THR values than the difunctional cyanate ester resins, but the dependence of THR on conversion (i.e. T_g) also seems to be lower as the curves for the PT-resins are closer together than for the di-functional resins. This has the practical implication that not fully cured PT-resins may fulfil aerospace FST requirements for interior parts.

However, more important is the fact that for FST-behaviour, modifications of cyanate esters with BA yield similar trends to those observed when varying conversion, see Figs. 27-29. The modification of B10 with BA leads to a broad distribution of THR curves similar to the variation of conversion in Fig. 23, whereas the BA-modified PT-resins fall more closely together with the neat PT-resins (Figs. 28 and 29) similar to the effect of conversion seen in Figs. 25 and 26. Modification with phenolic components is especially interesting for PT-resins, since the curing temperature needed to reach T_g(max) is reduced significantly. As there is only a small influence of phenolic modification on the FST properties of the PT-resins, it is possible to formulate FST-resins with good processibility and low flammability.

3.3 Toughening with Low Molecular Weight PES

The PT-resins exhibit good FST properties, so it is of interest to compare the toughening of PT15 and B10 with a low flammability high-T_g amorphous thermoplastic such as polyethersulphone (PES). B10 serves as the control, as many reports in the

ACCEPTED MANUSCRIPT

literature have investigated TP-toughening of B10 only. PT15 has the lowest viscosity of the commercially-available PT-resins (PT15, PT30, PT60, PT90), so is especially suitable for infusion techniques. The FST-properties of PT15 are not as good as those of PT30, but are much better than those of the di-functional cyanate esters (see above). This combination of relatively low viscosity and good FST properties led to PT15 being chosen as the second matrix resin for toughening with PES.

The dynamic viscosity of 20% PES in PT15 is shown in Fig. 30 for all synthesized PES as a function of the molecular weight (M_n) of the respective PES grade. There is a steep rise of viscosity with increasing M_n of PES, showing an approximately linear relationship in a logarithmic plot. This steep rise, together with the equally steep rise with content of PES in PT15 (see Fig. 31), shows that a balance of properties has to be found if low viscosity formulations are to be developed using PES as a toughening agent.

The fracture toughness values for B10 and PT15 modified with different contents of PES are compared in Fig. 32. Four types of synthesized PES with molecular weights between 3000 and 10500 (M_n), and one commercial high molecular weight (HMW) type (M_w ~35000), were used. Three of these PES grades have been used only in one of the cyanate esters, but two (M_n 5251 and 7123) can be compared directly. The toughening effect is higher for PT15 than for B10 using both grades of PES. This is because the tendency to phase separate is stronger for PT15, as this novolac-type molecule is less compatible than B10 with the PES used here. The DMA curves for B10 and PT15 modified with different contents of these two PES grades are compared in Fig. 33. The peak for the PES glass transition is more distinct with PT15, indicating a higher degree of phase separation. Further evidence is seen from TEM, and example micrographs are shown in Fig. 34 for PT15 modified with the M_n-5251 PES grade. For 10% of PES a particulate morphology is seen with PES being the particulate phase, whereas for 15 and 20% a co-continuous morphology is formed. Transmission electron micrographs for B10 modified with the same M_n-5251 PES showed no clear signs of phase separation (not shown here).

Even with the higher molecular weight PES (M_n 7123) the increase in fracture toughness is relatively low for PT15. The fracture toughness of B10 modified with this PES grade with M_n around 10500 approaches the curve for B10 with a HMW commercial type (UDEL P-1800), but still the fracture toughness with the synthesized

ACCEPTED MANUSCRIPT

M_n-10500-PES is lower. Since the toughening effect is higher for PT15 modified with the lower molecular weight PES grades than for B10 with the same PES grades, it can be expected that the toughening effect for PT15 modified with the M_n-10500 PES grade would be even higher than that for B10 modified with this PES grade. (There was not enough PES-10500 available to check this.) These results highlight the importance of tailoring the chemical structure and molecular weight of the TP toughening agent specifically for each resin monomer in order to achieve an optimum balance of processing and fracture properties.

The singular importance of toughening of highly-crosslinked and thus high-T_g resins such as PT15 by high-T_g TP is further illustrated in Fig. 35. In this graph unpublished results of many different investigations of the authors have been summarized as a plot of fracture toughness over T_g. The points in this graph can be divided into two groups according to whether they use rubber or thermoplastic toughening.

Rubber toughening. This is defined as modification with soft rubbery particles (which may be core-shell particles or phase-separating liquid rubbers with aliphatic silicone as well as organic (such as butadiene) chains). The efficiency of rubber toughening depends on the ductility of the matrix, consequently for highly crosslinked matrix resins with a high T_g (which are much less ductile than low T_g resins) the effect of rubber toughening is drastically reduced, as is indicated by the enveloping curve in Fig. 35.

Thermoplastic toughening. For high-T_g amorphous thermoplastics there is a different toughening mechanism. The toughening effect is simply controlled by rules of mixture, and the condition for a high toughening effect is that the thermoplastic phase controls the toughness of the blend, which is achieved at high TP-contents by a co-continuous phase morphology. Thus thermoplastic toughening can be applied also to very brittle highly-crosslinked high-T_g resins such as PT15, because the toughening effect is independent of the ductility of the resin phase, it only depends on the volume and morphology of the thermoplastic phase. Thus, high toughness and high T_g can be achieved simultaneously. This is clearly seen in Fig. 35 where the points for PT15 modified with high-T_g thermoplastics fall into a field indicated by the vertical ellipse. These are the only points that fall outside the enveloping curve for rubber toughening, which illustrates that thermoplastic toughening is controlled by a different toughening mechanism. Most of these points with very high fracture toughness and high T_g are cyanate esters modified with commercial high-T_g TPs (such as ULTEM 1000, UDEL P-

ACCEPTED MANUSCRIPT

1800 and some other commercial types as described in [52]). In principle toughening with lower molecular weight grades of high-T_g thermoplastics (as investigated here) falls into this group. However, the increases in toughness achieved so far were not as high as with the commercial high molecular weight TPs, therefore points for synthesized lower molecular weight grades do not stick out so clearly from the field for rubber-toughened thermosets.

TP-toughening is currently the only way to achieve a very high T_g combined with high toughness. The problem is that a relatively high viscosity has to be accepted, and all measures to reduce viscosity (such as using low molar mass grades or low contents of TP) reduce the toughening effect. Recently, low viscosity block-co-polymers have been developed which have a significant toughening effect in some di-functional cyanate ester resins, and some toughening is achieved in PT-resins. The viscosity increases only slightly, even more so because only a low content of toughening agent (~5%) is needed to achieve a significant toughening effect [53].

3.4 Water uptake

Long-term water uptake data at 28°C, 50°C (for some of the cyanate esters) and 70°C are shown in Figs. 36-40 as a function of normalized square root of time $t^{-1/2}/l$ (where l is the thickness of the specimens), for B10, M10, XU366, XU71787.02 and PT15 with different conversions. Distinctly non-Fickian water uptake behaviour occurs at 70°C for all of the cyanate esters. However, closer analysis shows that at 28°C none of the data can be described completely by a Fickian diffusion law, i.e. there is some non-Fickian water uptake even at 28°C. Thus, the Fickian equilibrium uptake cannot be determined by extrapolation of long-term data to infinity, as could be done for purely Fickian behaviour.

To separate the non-Fickian from the Fickian water uptake, an estimate for the Fickian equilibrium uptake value has been obtained by taking the value at $t^{1/2}/l = 0.5*10^6$ $s^{1/2}/m$ (approximately 150 h for samples that are 1.5 mm thick)). This is the time where a short Fickian plateau is observed for at least some of the cyanate esters before the non-Fickian uptake becomes visible. These points are shown as open symbols in Figs. 36-40. The non-Fickian part of the uptake is calculated as the total uptake minus the estimated Fickian equilibrium uptake. The total uptake is determined at $t^{1/2}/l = 3.2 \times 10^6$ $s^{1/2}/m$ (approximately at 6400 h for samples that are 1.5 mm thick). Although there is

ACCEPTED MANUSCRIPT

clearly some error and arbitrariness involved with such a procedure, it illustrates the main trends and the underlying mechanisms. The non-Fickian uptake is plotted versus the estimated Fickian equilibrium uptake in Fig. 41, for all the cyanate esters investigated. The numbers by the symbols are the respective conversions. It is not surprising that the non-Fickian uptake is proportional to the Fickian uptake in general. This is because non-Fickian uptake is supposed to be driven by hydrolytic degradation of the network, which can be described as an equilibrium reaction: The higher the concentration of the reaction partner (water), the more the hydrolytic degradation is accelerated. However, some of the trends with temperature and conversion are more complex. It is interesting to look more closely at the water uptake data for M10 (TMDCBF) and B10 (DCBA) in Fig. 41. The non-Fickian uptake increases with increasing conversion for uptake at 28°C for both B10 and M10. However, the slope is higher for M10 (TMDCBF) than for B10 (DCBA). This clearly supports the free volume interpretation given in Section 3.1 above. Free volume alleviates the transport of reaction products and the hydrolytic reaction itself, so the higher free volume of M10 (TMDCBF) leads to a higher non-Fickian uptake and a higher dependence on conversion. This also explains why the estimated Fickian equilibrium uptake is lower for M10 than for B10 (as can be expected because the backbone structure of M10 is more hydrophobic (methyl groups in ortho-position) than that for B10) but the non-Fickian part of uptake is higher for M10. Very likely it is the free volume which is supposedly higher for M10 (TMDCBF) than for all other polycyanurate networks which accounts for this deviation in case of M10 from the proportionality between the Fickian and non-Fickian part which is seen for all other polycyanurates.

The fact that the free volume dependence on conversion increases the non-Fickian uptake at 28°C but there is a reversed trend at 70°C for both B10 and M10 can be explained by the dependence of T_g on conversion. At a storage temperature of 70°C the T_g of the specimens with low conversions are not much higher than the water temperature. Furthermore, the higher the uptake the more that T_g is reduced, i.e. this so-called T_g(wet) decreases with water uptake time. The reverse trend (i.e. that the non-Fickian uptake falls with conversion for B10 and M10 at 70°C, whereas it rises with conversion at 28°C) can be explained by the near T_g for low conversions: The influence of the difference between T_g(wet) and the water storage temperature dominates the influence of free volume at 70°C. For the lowest conversions this

ACCEPTED MANUSCRIPT

difference is the smallest, and thus molecular mobility is significantly increased which accelerates hydrolytic degradation. On the other hand, for high conversions the network is still in the glassy state (T_g and also T_g (wet) are much higher than the water storage temperature), thus hydrolytic degradation is postponed and the non-Fickian uptake is reduced.

The T_g of PT15 is higher than for B10 and M10, so at 70°C storage temperature the free volume effect dominates with PT15, and non-Fickian uptake rises with conversion at both 28°C and 70°C. XU366 has the lowest T_g of all the polycyanurates, and therefore at 28°C the T_g effect dominates over the free volume effect. Therefore the non-Fickian uptake values for all storage temperatures fall with conversion for XU366. The decrease is much stronger at 70°C water storage temperature, which supports the T_g explanation. For XU71787.02 there seems to be a reversion of the trends along the curve for the 70°C uptake. For low conversions (from 76 to 88% conversion) the free volume effect is dominant (which leads to an increase of the non-Fickian uptake with conversion). Above 88% conversion the effect of T_g becomes dominant, so at conversions higher than 88% the non-Fickian uptake decreases with conversion. This fits well to the fact that the T_g of XU71787.02 lies between that of XU366 and those of B10 and M10.

The explanation of non-Fickian diffusion behaviour in polycyanurates by hydrolytic degradation is largely accepted and substantiated in the literature [37,44-47]. It has been reported that T_g after redrying decreases (compared to the T_g of the network before water immersion) as a consequence of hydrolytic degradation of the network. This effect was also found in the present work: Specimens with full conversion (in order to avoid mixing of post-curing and hydrolytic degradation effects) were redried after long-term immersion in water and tested using DMA. The T_g values of the redried samples are plotted as a function of the water storage temperature in Fig. 42. (Note that the value for T_g at T = 0 is the value for the sample before storage, not for 0°C water storage.) It is seen that degradation indicated by a drop in T_g is accelerated at water storage temperatures higher than 50°C, whereas it remains relatively moderate below 50°C. As can be expected, the drop in T_g, (i.e. the difference between the initial T_g and the T_g after storage and redrying) is nearly proportional to the non-Fickian water uptake for all cyanate esters, see Fig. 43, with the exception of M10. However,

ACCEPTED MANUSCRIPT

the points do not fall on one line for all of the cyanate esters. The sensitivity to hydrolytic degradation can be defined as the slope of curves in Fig. 43, where the steeper curves indicate a higher sensitivity to hydrolytic degradation. This sensitivity to hydrolytic attack seems to be by far the highest for B10 and M10, as indicated by the steepest slopes (the curve for M10 being even steeper than that for B10). The sensitivity for PT15 is not as high as that for B10, although PT15 shows the highest non-Fickian (as well as total) uptake. The slope for PT15 is even lower than that for XU71787.02 and XU366, which both fall on one line.

Measuring the T_g drop as an indicator for hydrolytic degradation seems to be a better approach than measuring the water uptake by measuring weight gain, because there are uncertainties when calculating non-Fickian uptake from the water uptake curves whereas the T_g drop can be measured quite accurately.

This work has shown the sensitivity of polycyanurates to hydrolytic degradation. However, it should be kept in mind that this is a long-term effect measured after about two years of immersion in water at moderate temperatures (28°C, 50°C, 70°C), and such a long-term immersion in water is not a realistic scenario for most applications. There are indications that free volume promotes hydrolytic degradation, which may lead to formulation strategies for cyanate esters. If the free volume can be reduced by formulating cyanate esters then their sensitivity to hydrolytic degradation may also be reduced. Alternatively, this may serve as an explanation as to why combinations of cyanate esters with some co-monomers significantly reduce their sensitivity to hydrolytic degradation.

4 Conclusions

In the first part of this work, dynamic mechanical analysis using a high precision torsional pendulum and density measurements were performed on polycyanurate networks from two different cyanate ester monomers cured to different conversions. The intensity of the γ-relaxation at about -100°C increased with conversion, whereas the shape and peak temperature remained largely unaffected. This was explained as an effect of frozen-in free volume, which increases with increasing conversion. Packing of the polycyanurate network with the more sterically-hindered backbone chain structure is hindered when cooling down through the γ-relaxation, resulting in a lower storage modulus at -189°C. In accordance with literature, the measured

ACCEPTED MANUSCRIPT

decrease of density with increased conversion was also attributed to the increased free volume frozen in as a consequence of the higher T_g with higher conversion. Fracture toughness measurements for these two cyanate esters indicated a brittle-ductile transition, where above a critical conversion there seems to be a sudden transition from extremely brittle to ductile behaviour.

In the second part, this brittle-ductile transition was studied in more detail for five different cyanate ester resins using a newly-developed optical crack tracing technique to measure fracture toughness very accurately. The existence of this transition was confirmed, and fracture toughness in the brittle range is as low as $K_{Ic} = 0.1$ MN*m$^{-3/2}$. The measured values of T_g were used as a measure of conversion, and the brittle-ductile transition is located at different T_g for the resins investigated. This is explained by a critical connectivity of the network where this transition takes place, and which is controlled by the backbone structure of the polycyanurate network. The effect of conversion on fracture toughness in the ductile range (i.e. above the brittle-ductile transition) depends on the toughness of the fully-cured cyanate. For the more brittle multifunctional PT-resins there is no significant effect of conversion on fracture toughness, whereas a significant effect is seen for the more ductile di-functional cyanate esters. This is explained by a correlation between the width and uniformity of the glass transition with the fracture toughness, which is also seen for other thermosets. Bisphenol-A modification (and phenolic modification in general) represents a route to modify the network structure of polycyanurates in a way similar to conversion and was used here for comparison. The effect of bisphenol-A modification on the mean value of fracture toughness is similar to that of conversion. However, co-curing cyanate esters with bisphenol-A seems to produce macroscopic fluctuations of the network structure causing a significant intrinsic variation of the fracture toughness.

Flammability was studied using cone calorimetry for five different cyanate esters with different conversions, as well as modifications of these with bisphenol-A. Higher conversions, and lower bisphenol-A content, reduces the heat release rate and shifts the curves to longer times. However, the effects of conversion and bisphenol-A modification are relatively small for the multifunctional PT-resins.

In the third part of this work, toughening of two different cyanate esters (dicyanate from bisphenol-A and a novolac-type cyanate) by bisphenol-A polyethersulphone (PES)

ACCEPTED MANUSCRIPT

was investigated, where the molecular weight of PES was varied between 3000 and 10500 (M_n). Higher toughening effects were found for the PES-toughened novolac-type cyanate. A certain molecular weight of PES toughening agent and contents higher than 20% are needed to achieve a significant toughening effect. However, this molecular weight can be lower than most of the commercially-available amorphous high-T_g thermoplastic toughening agents.

In the fourth and last part of this work, the long-term water uptake (over two years) was studied at moderate temperatures (28°C, 50°C, 70°C) for five different cyanate esters with different conversions. Non-Fickian water uptake behaviour was observed for all the cyanate esters investigated, even at water storage temperatures as low as 28°C. The non-Fickian water uptake (which is attributed to hydrolytic degradation) was separated from the estimated Fickian equilibrium uptake. This non-Fickian uptake is roughly proportional to the estimated Fickian equilibrium uptake. It is also proportional to the T_g-drop as defined by T_g(fresh) – T_g(redried after water storage), however the sensitivity to hydrolytic degradation as defined by the slope of this proportionality is quite different for the different cyanate esters. Conversion has a complex effect on non-Fickian water uptake. At low water storage temperatures free volume effects seem to dominate, whereas at higher water uptake temperatures the lower T_g for lower conversion and thus increased molecular mobility seem to dominate over the free volume effects, at least for the high-T_g polycyanurates.

These results form an answer to the question whether cyanate esters could be used in structural applications at conversions lower than the maximum conversion. Considering the brittle-to-ductile transition in toughness then cyanates have to reach a critical conversion to be safely in the ductile state. To allow for a safety margin the conversion should be higher than 80%. Considering flammability, cyanate esters with higher conversion exhibit lower flammability, i.e. lower heat release. However, even at low conversions (~80%) the heat release of cyanate esters is much lower than that of epoxies and epoxy-cyanates. Thus, aerospace flammability requirements are very likely to be fulfilled at lower conversions (>80%), especially with the PT-resins. Hydrolysis could be a problem with pure polycyanurate networks. However, the dependence of hydrolytic sensitivity on conversion is relatively low (for some cyanates lower conversions even reduce the hydrolytic sensitivity somewhat, for others it is slightly increased with conversion). Conversion is not the main factor for hydrolysis, it

ACCEPTED MANUSCRIPT

is the Fickian equilibrium water uptake of the network which has to be reduced, and this is influenced largely by the chemical backbone structure. Co-reactions with monomers of low polarity such as siloxane-containing building blocks are likely to reduce hydrolysis to a level which is acceptable for safety-critical applications.

5 Acknowledgements

This work was supported by the European Commission (BriteEuram-Project No BE-96-3947) and by the German Ministry of Economy (LUFO III, KATO-Neue Werkstoffe für Sandwich- und Klebstoff-Anwendungen, 2003-2006, 20K0302T). The authors thank Iris Geike and Karin Göcks for preparing samples, Daniela Meikofski for synthesis of PES grades, Prof. Frank Kuschel for supervising the synthesis work, Joachim Müller for torsional pendulum measurements, Thomas Mühlenberg for cone calorimeter measurements, and Oliver Brandl for carrying out the density measurements.

6 Literature

[1] I. Hamerton (Ed.), Chemistry and Technology of Cyanate Ester Resins, Blackie Academic, Glasgow, 1994.

[2] J. Bauer, M. Bauer, C. Uhlig, Quick-setting mixtures and kits with polyfunctional cyanates and amines, the thermosets produced therefrom and methods for the production thereof, Patent EP 1 265 947 B1, Patent US 6,822,067 B2.

[3] A. Snow, J.P. Armistead, J. Appl. Polym. Sci. 52 (1994) 401-411.

[4] O. Georjon, J. Galy, Polym. Mater. Sci. Eng. 71 (1994) 754-755.

[5] O. Georjon, J. Galy, J. Appl. Polym. Sci. 65 (1997)2471-2479.

[6] O. Georjon, G. G. Schwach, J.-F. Gerard, J. Galy, J. Albrand, Polym. Eng. Science 37 (1997) 1606-1620.

[7] O. Georjon, J. Galy, Polymer 39 (1998) 339-345.

[8] M. Bauer, C. Uhlig, J. Bauer, S. Harris, D. Dixon, in B.T. Stokke and A. Elgsaeter, Eds., Wiley Polymer Network Group Review Series Vol. 2, 1999 John Wiley & Sons Ltd, pp. 271-283.

[9] C. Uhlig, O. Kahle, B. Wieneke, M. Bauer, Optical Crack Tracing – A New Method for the Automatic Determination of Fracture Toughness of Polymers,

ACCEPTED MANUSCRIPT

Proceedings MicroMat 2000, 618-629 and Forum der Forschung, 11 (2000) 50-53.

[10] R.E. Lyon, R.N. Walters, S. Gandhi, Fire and Materials 30 (2006) 89-106.

[11] R.N. Walters, R.E. Lyon, Covina, Ca., SAMPE International Business Office, 2007, Paper 80, pp.12, CD-ROM. 012

[12] R.E. Lyon, L. Speitel, R. Filipczak, R.N. Walters, S. Crowley, S. Stoliarov, L. Castelli, M. Ramirez, High Perform. Polym. 19 (2007) 323-355.

[13] D. Zhuo, A. Gu, G. Liang, J.-T. Hu, L. Cao, L. Yuan, Polym. Degrad. Stab. 96 (2011) 505-514.

[14] M. Bauer, J. Bauer, „Networks from dicyanate of bisphenol A and diphenols.“; Networks 90, Jerusalem 1990.

[15] M. Bauer, J. Bauer, S. Jährig; Makromol. Chem., Macromol. Symp. 45 (1991) 97-106

[16] J. Bauer, C. Alla, M. Bauer, B. Bloch, Acta Polym. 46 (1995) 241-246.

[17] J.Y. Chang, J.-L. Hong, J. Polym. Res. 4 (1997) 203-211.

[18] J.-Y. Chang, J.-L. Hong, Polymer 42 (2001) 1525-1532.

[19] G. Zhan, S. Hu, Y. Yu, S. Li, X. Tang, J. Appl. Polym. Sci. 113 (2009) 60-70.

[20] J.W. Hwang, S.D. Park, K. Cho, J.K. Kim, C.E. Park, T.S. Oh, Polymer 38 (1997) 1835-1843.

[21] J.-Y. Chang, J.-L. Hong, Polymer 41 (2000) 4513-4521.

[22] J.W. Hwang, K. Cho, T.H. Yoon, C.E. Park, J. Appl. Polym. Sci. 77 (2000) 921-927.

[23] J.W. Hwang, K. Cho, C.E. Park, W. Hoh, J. Appl. Polym. Sci. 74 (1999) 33-45.

[24] R.W. Hillermeier, J.C. Seferis, J. Appl. Polym. Sci., 77 (2000) 556-567.

[25] J.N. Suman, J.K. Kathi, S. Tammishetti, European Polym. J. 41 (2005) 2963-2972.

[26] S.A. Srinivasan, J.E. McGrath, Polymer 39 (1998) 2415-2477.

[27] Z. Cao, F. Mechin, J.-P. Pascault, Polym. Int. 34 (1994) 41-48.

[28] M. Thunga, M. Akinc, M.R. Kessler, eXPRESS Polym. Letters 8 (2014) 336-344.

[29] C.M. Gomez, I. Porcar, I. Recalde, A. Campos, Polym. Int. 52 (2003) 1480-1486.

[30] S.A. Srinivasan, J.E. McGrath, High Perform. Polym. 5 (1993) 259-274.

[31] I.E. Recalde, A. Campos, I. Mondragon, C.M. Gomez, Macromol. Symp. 174 (2001) 175-185.

ACCEPTED MANUSCRIPT

[32] A.V. Rau, S.A., Srinivasan, J.E. McGrath, A.C. Loos, Polym. Compos. 19 (1998) 166-179.

[33] S.A. Srinivasan, J.E. McGrath, J. Appl. Polym. Sci. 64 (1997) 179-190.

[34] G. Wang, R. Wang, G. Fu, T. Gao, C. Fu, H. Kuang, F. Yang, W. Jiao, L. Hao, W. Liu, Polym. Eng. Sci. 55 (2015) 2591-2602.

[35] D.H. Wertz, D.C. Prevorsek, Polym. Eng. Sci. 25 (1985) 804-806.

[36] T.J. Wooster, S. Abrol, D.R. MacFarlane, Macromol. Mater. Eng. 290 (2005) 961-969.

[37] L.J. Kasehagen, I. Haury, W. Macosko, D. A. Shimp, J. Appl. Polym. Sci. 64 (1997) 107-113.

[38] S.K. Karad, F.R. Jones, Polymer 46 (2005) 2732-2738.

[39] S.K. Karad, F.R. Jones, D. Attwood, Polymer 43 (2002) 5643-5649.

[40] S.K. Karad, D. Attwood, F.R. Jones, Composites: Part A 33 (2002) 1665-1675.

[41] S.K. Karad, D. Attwood, F.R. Jones, Polym. Composites 24 (2003) 567-676.

[42] S.K. Karad, D. Attwood, F.R. Jones, Composites: Part A 36 (2002) 764-771.

[43] A.J. Guenther, M.E. Wright, A.P. Chafin, J.T. Reams, K.R. Lamison, M.D. Ford, S.P.J. Kirby, J.J. Zavala, J. M. Mabry, Macromolecules 47 (2014) 7691-7700.

[44] A. Chaplin, I. Hamerton, H. Herman, A.K. Mudhar, S.J. Shaw, Polymer 41 (2000) 3945-3956.

[45] V. V. Marella, J. A. Throckmorton, G.R. Palmese, Polym. Degrad. Stab. 104 (2014) 104-111.

[46] E. Kollia, Th. Loutas, E. Fiamegkou, A. Vavouliotis, V. Kostopoulos, Polym. Degrad. Stab. 121 (2015) 200-207.

[47] I. Hamerton, H. Herman, K.T. Rees, A. Chaplin, S.J. Shaw, Polym. Int. 50 (2001) 475-483.

[48] M. Bauer, J. Bauer, in I. Hamerton (Ed.), Chemistry and Technology of Cyanate Ester Resins, Blackie Academic, Glasgow, 1994, pp. 59-86.

[49] ASTM D4045-99, ISO 13586-1.

[50] I.M. Ward, Mechanical Properties of Solid Polymers, Wiley-Interscience, London 1971 (first edition), chapter 5.

[51] Publication in progress.

[52] C. Uhlig, M. Bauer, J. Bauer, New Cyanate Materials, BriteEuram-Project No BE-96-3947, Final Report (2000).

ACCEPTED MANUSCRIPT

[53] C. Uhlig, M. Bauer, Cyanate-based resins with reduced viscosity and duromers produced therefrom with improved impact resistance, Patent EP 2 714 774 A (29.05.2012), US 2014/ 0199906 A1 (29.05.2012).

ACCEPTED MANUSCRIPT

ACCEPTED MANUSCRIPT

Figure captions

Fig. 1: Optical crack tracing (OCT) technique: measured data (P(t) and a(t)) (left), and R-curve from fracture mechanics analysis (K_{Ic}(a) and G_{Ic}(a)) (right).

Fig. 2: left: R-curve for a specimen with an imperfect pre-crack (green curve) showing a too-high K_{Ic} for initiation and R-curves for nearly-perfect pre-cracks (blue and magenta curves); upper right image: mapped crack plane with an imperfect (twisted) pre-crack, lower right image: mapped crack plane for a nearly-perfect pre-crack.

Fig. 3: Torsional pendulum DMA measurements for M10 (TMDCBF) cured to different conversions.

Fig. 4: Torsional pendulum DMA measurements for B10 (DCBA) cured to different conversions.

Fig. 5: T_g versus conversion for B10 (DCBA) and M10 (TMDCBF).

Fig. 6: Density versus conversion for B10 (DCBA) and M10 (TMDCBF).

Fig. 7: Storage modulus G' (at 25°C, data from Figs. 3 and 4) versus density (data from Fig. 6) for B10 (DCBA) and M10 (TMDCBF).

Fig. 8: Peak height of γ-relaxation (log(tan δ) (data from Figs. 3 and 4) versus conversion for B10 (DCBA) and M10 (TMDCBF).

Fig. 9: Storage modulus G' (at -189°C and 25°C, data from Figs. 3 and 4) versus conversion for B10 (DCBA) and M10 (TMDCBF).

Fig. 10: Fracture toughness (critical stress intensity factor K_{Ic}) versus conversion for B10 (DCBA) and M10 (TMDCBF).

Fig. 11: Fracture toughness (critical stress intensity factor K_{Ic}, same data as Fig. 10) versus T_g for B10 (DCBA) and TMDCBF (M10).

Fig. 12: DMA curves for XU366 cured to different conversions.

Fig. 13: DMA curves for L10 cured to different conversions.

Fig. 14: DMA curves for B10 cured to different conversions. Open symbols indicate how T_g was determined for broad tan δ peaks by fitting a model tan δ peak (see text for further explanation).

Fig. 15: DMA curves for PT15 cured to different conversions.

Fig. 16: DMA curves for PT30 cured to different conversions.

Fig. 17: Fracture toughness (critical stress intensity factor K_{Ic}) versus T_g (as a measure of conversion) for five different cyanate esters.

ACCEPTED MANUSCRIPT

Fig. 18: Fracture toughness (critical stress intensity factor K_{Ic}) versus T_g (as a measure of conversion) for B10 modified with different contents of bisphenol-A (BA). (Error bars represent an intrinsic variation of fracture toughness, not experimental error.)
Fig. 19: Fracture toughness (critical stress intensity factor K_{Ic}) versus T_g (as a measure of conversion) for four different cyanate esters modified with different contents of bisphenol-A (BA) – contents between 5 and 20%. (Error bars represent an intrinsic variation of fracture toughness, not experimental error.)
Fig. 20: Heat release rate (HRR) curves for B10, various castings measured to assess reproducibility, all castings cured with the same curing cycle (max. cure temperature 280°C).
Fig. 21: Total heat release (THR), integral of HRR data from Fig. 20.
Fig. 22: THR for XU366 cured to different conversions (T_g given as a measure of conversion).
Fig. 23: THR for B10 cured to different conversions (T_g given as a measure of conversion).
Fig. 24: THR for L10 cured to different conversions (T_g given as a measure of conversion).
Fig. 25: THR for PT15 cured to different conversions (T_g given as a measure of conversion).
Fig. 26: THR for PT30 cured to different conversions (T_g given as a measure of conversion).
Fig. 27: THR for neat B10 and B10 modified with BA (T_g given as a measure of conversion).
Fig. 28: THR for neat PT15 and PT15 modified with BA (maximum curing temperature given in legend).
Fig. 29: THR for neat PT30 and PT30 modified with BA (maximum curing temperature given in legend).
Fig. 30: Dynamic (complex) viscosity at 80°C versus molecular weight (M_n) of PES, for 20% PES in PT15.
Fig. 31: Dynamic (complex) minimum viscosity versus PES content in PT15, for one grade of PES.
Fig. 32: Fracture toughness (critical stress intensity factor K_{Ic}) versus PES content in PT15 and B10.

ACCEPTED MANUSCRIPT

Fig. 33: DMA curves for PT15 (left) and B10 (right) modified with two types of PES (upper row: M_n 7123, lower row: M_n 5251).

Fig. 34: TEM micrographs of PT15 modified with different contents of PES (M_n = 5251).

Fig. 35: Fracture toughness (critical stress intensity factor K_{Ic}) versus T_g for neat resins, rubber-toughened resins and resins toughened using high-T_g-amorphous thermoplastics (both high and low molecular weight (HMW, LMW)). All points for rubber toughening fall between the upper and lower curves (lower curve describes neat resins), whereas points for thermoplastic toughening of cyanate esters with highest toughness are indicated by the vertical ellipse. Data are from unpublished investigations of the authors.

Fig. 36: Water uptake versus normalized square root of time ($t^{-1/2}/l$) for PT15 with 91.7% and 98.4% conversion (left to right) at different storage temperatures.

Fig. 37: Water uptake versus normalized square root of time ($t^{-1/2}/l$) for M10 with 83.9%, 87.9%, 91.7% and 97.8% conversion (upper left to lower right) at different storage temperatures.

Fig. 38: Water uptake versus normalized square root of time ($t^{-1/2}/l$) for B10 with 83.9% and 87.9% conversion at different storage temperatures.

Fig. 39: Water uptake versus normalized square root of time ($t^{-1/2}/l$) for XU366 with 77.9%, 95.8%, 98.9% and 99.0% conversion (upper left to lower right) at different storage temperatures.

Fig. 40: Water uptake versus normalized square root of time ($t^{-1/2}/l$) for XU71787.02 with 76.3%, 88.0%, 89.9% and 95.9% conversion (upper left to lower right) at different storage temperatures.

Fig. 41: Non-Fickian part of total water uptake as versus estimated Fickian equilibrium uptake for all cyanate esters used (see text for explanation).

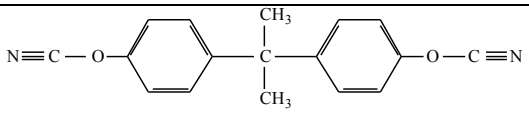
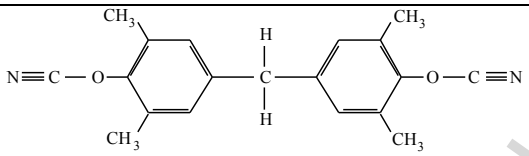
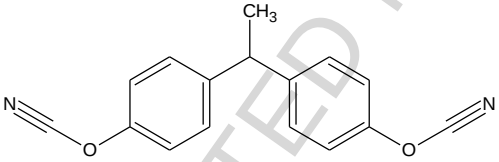
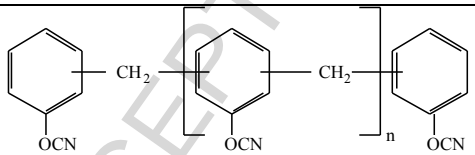
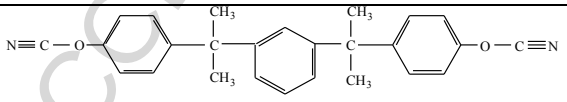
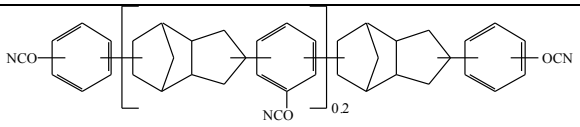
Fig. 42: T_g(redried) versus water storage temperature. Data at zero (on x-axis) represent initial T_g (before storage).

Fig. 43: T_g drop (= T_g(fresh) - T_g(redried after storage)) versus non-Fickian water uptake.

ACCEPTED MANUSCRIPT

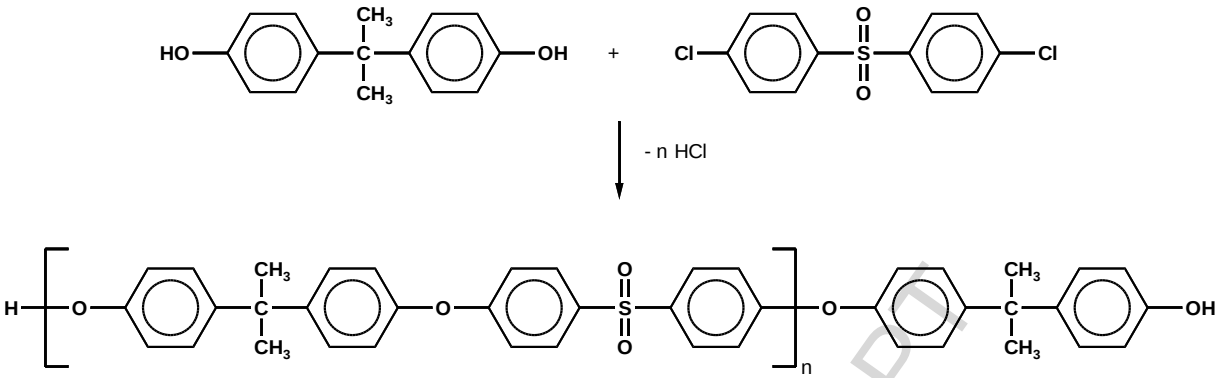
Tables

Table 1: Cyanates used

Code used	Chemical formula	Trade names and other names
B10, DCBA		AroCy B10 (Huntsman) BADCy (Lonza) 2,2'-bis(4-cyanatophenyl)propane 2,2'-bis(4-cyanatophenyl)isopropylidene Dicyanate of bisphenol A (DCBA) Bisphenol-A dicyanate (BADCy) RDX64826 (BPADCy) BT2000
M10, TMDCBF		AroCy M10 (Huntsman) METHYLCy (Lonza) Tetramethylbisphenol F dicyanate Tetramethyldicyanate from bisphenol F (TMDCBF) Methylene bis(3,5-dimethylphenyl-4-cyanate) bis(4-cyanato-3,5-dimethylphenyl)methane RDX64833 Dicyanate of tetramethylbisphenol F
L10		AroCy L10 (Huntsman) Primaset LECy (Lonza) 1,1-bis(4-cyanatophenyl)ethane 4,4'-Ethylidendiphenylcyanate
PT15, PT30		Primaset PT15, PT30 (Allied Signal, Lonza) Cyanated novolac
RTX366		AroCy XU 366 (Huntsman) RTX 366 (Rhone-Poulenc) 1,3-bis(4-cyanatophenyl-1-(1-methylethylidene)benzene 4,4'-[1,3-phenylene bis(1-methylethylidene)]bisphenol dicyanate Dicyanate of bisphenol M
XU-71787.02		XU-71787.02 (Dow-USA) Cyanate ester resin of phenol-dicyclopentadiene oligomer

ACCEPTED MANUSCRIPT

Schemes and Figures



Scheme 1: Synthesis route of linear bisphenol-A polyethersulphones (PES).

Figures

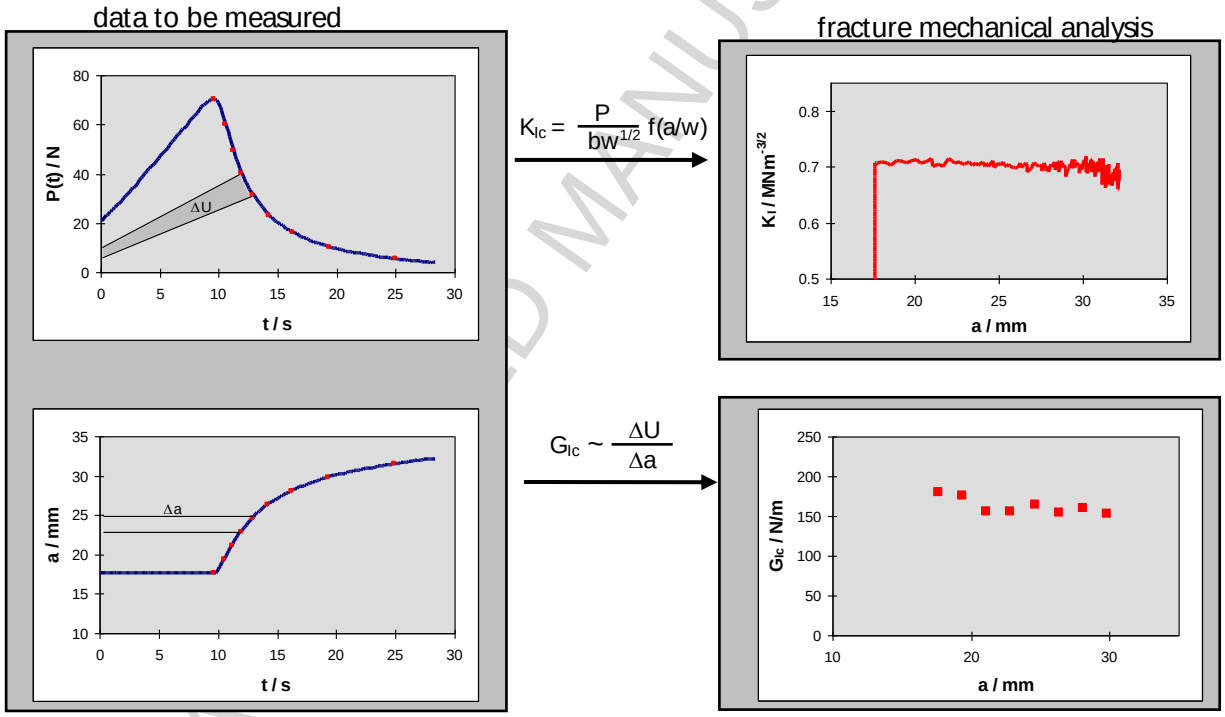


Fig. 1:

ACCEPTED MANUSCRIPT

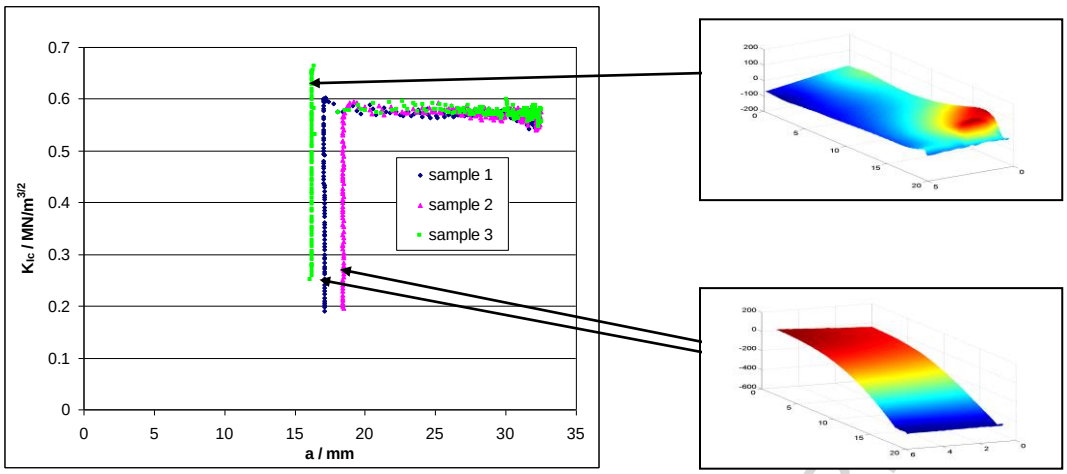


Fig. 2:

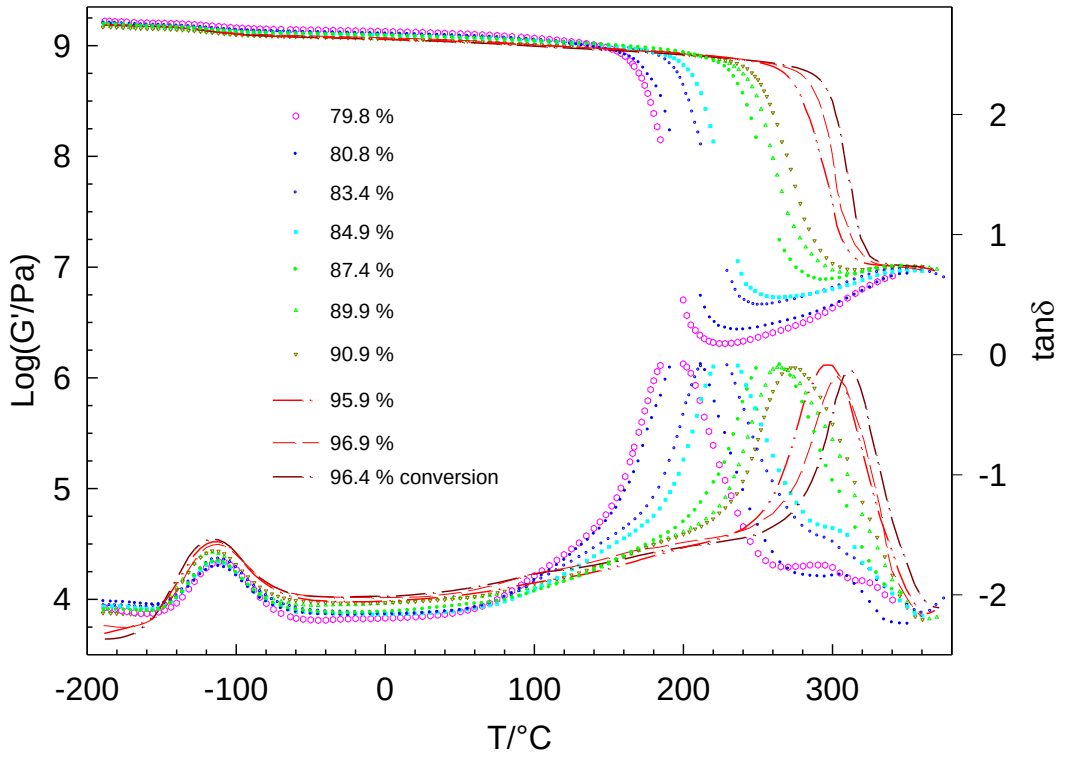


Fig. 3:

ACCEPTED MANUSCRIPT

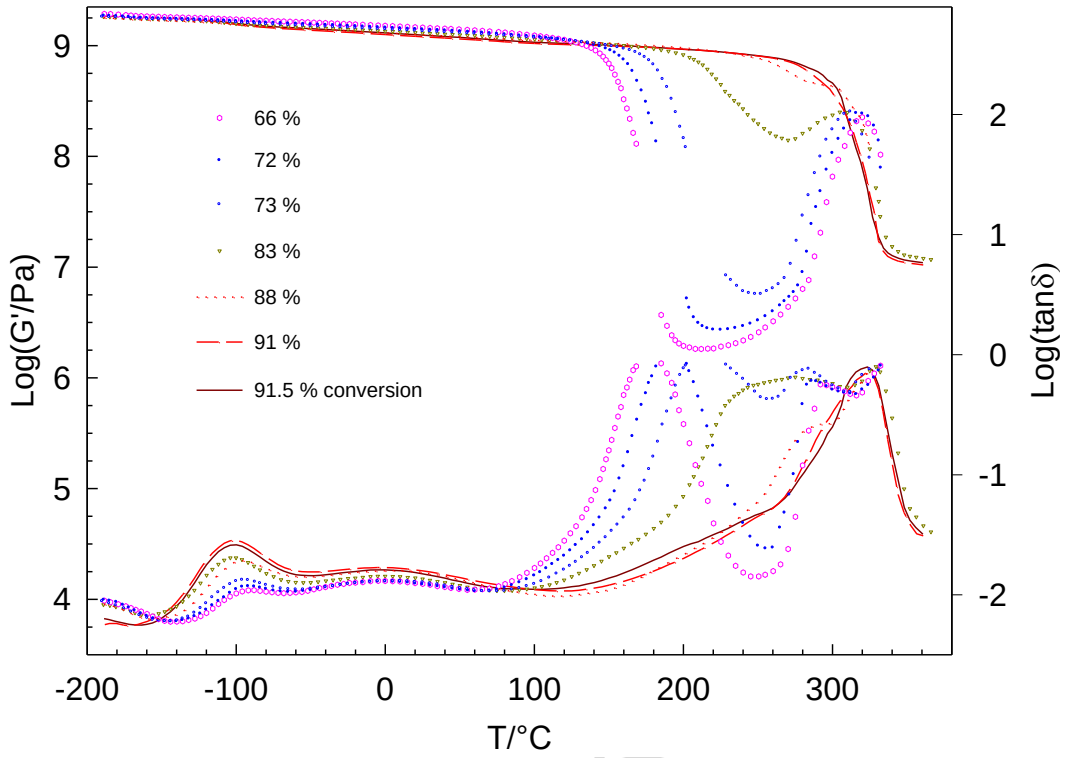


Fig. 4:

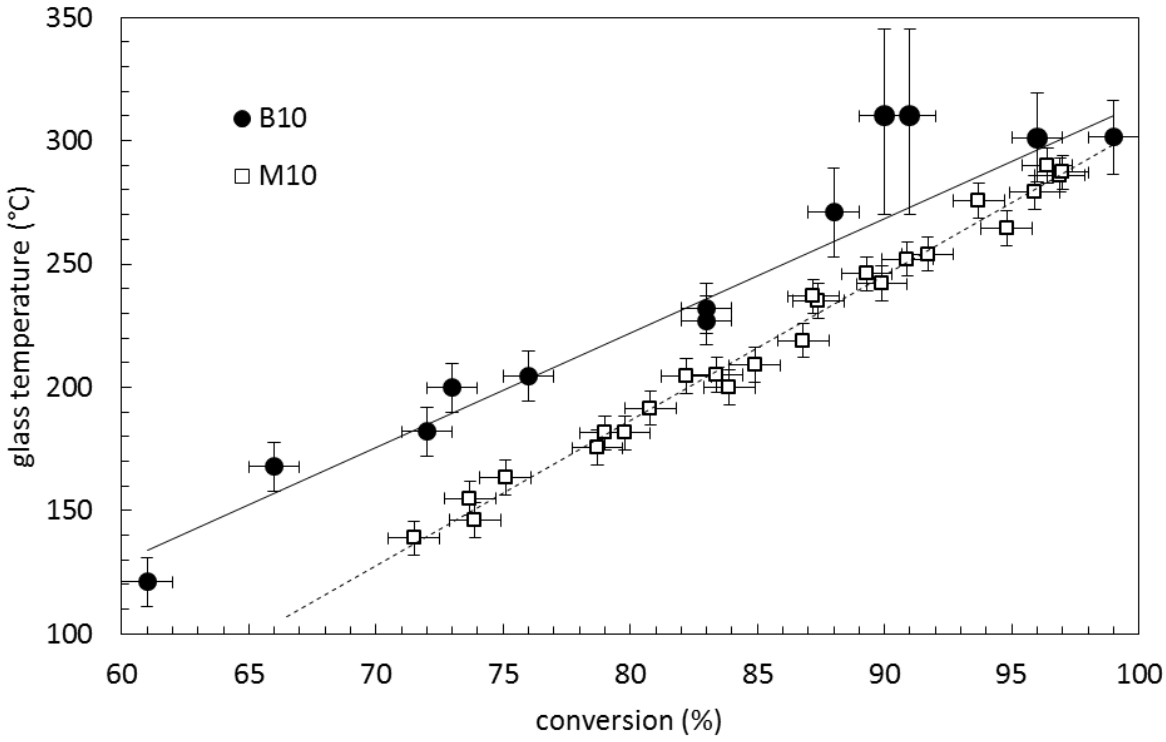


Fig. 5:

ACCEPTED MANUSCRIPT

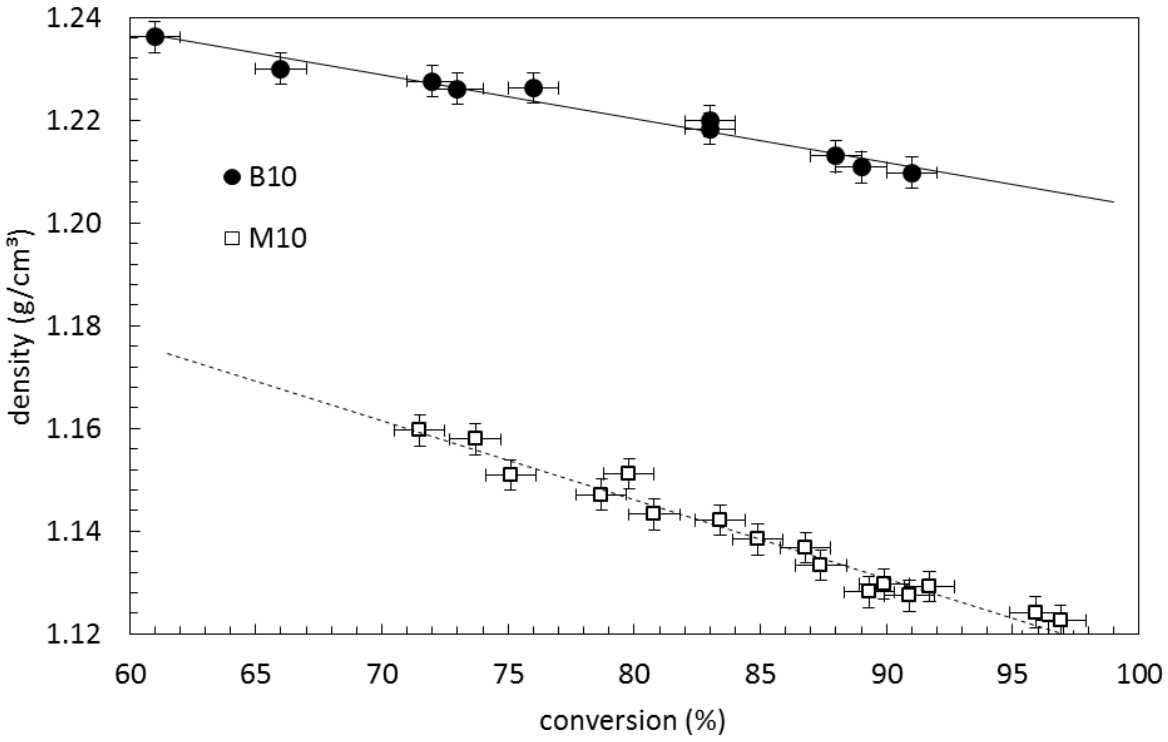


Fig. 6:

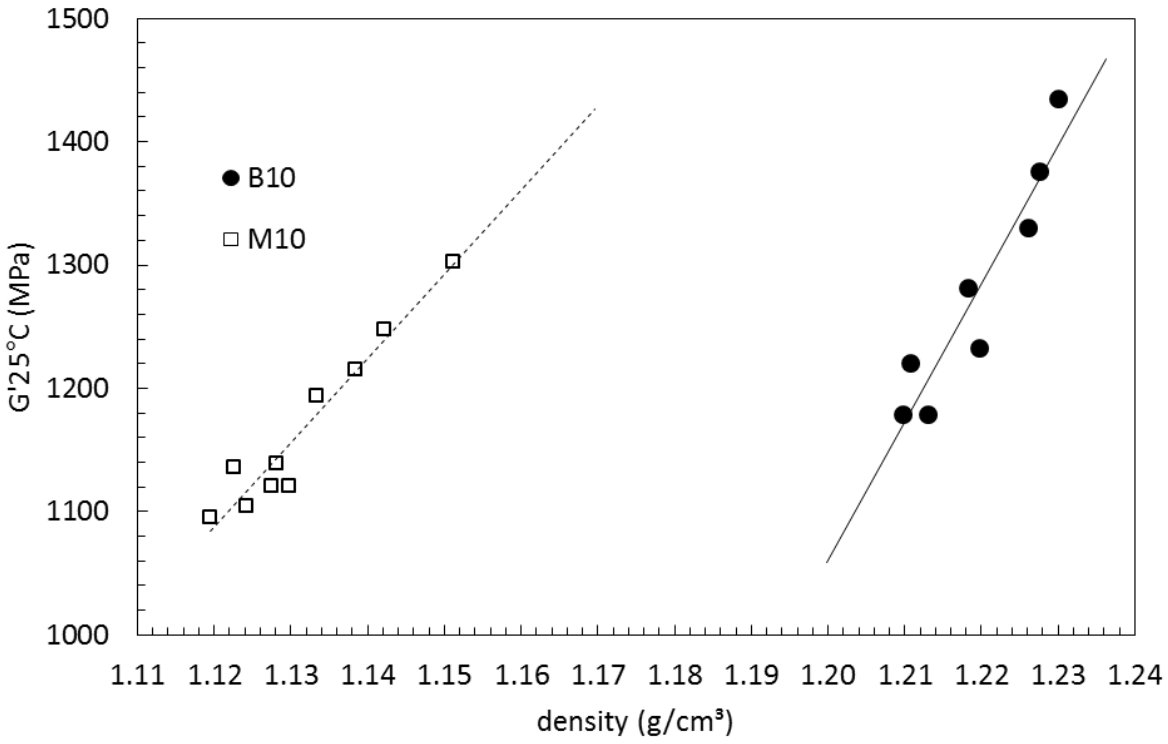


Fig. 7:

ACCEPTED MANUSCRIPT

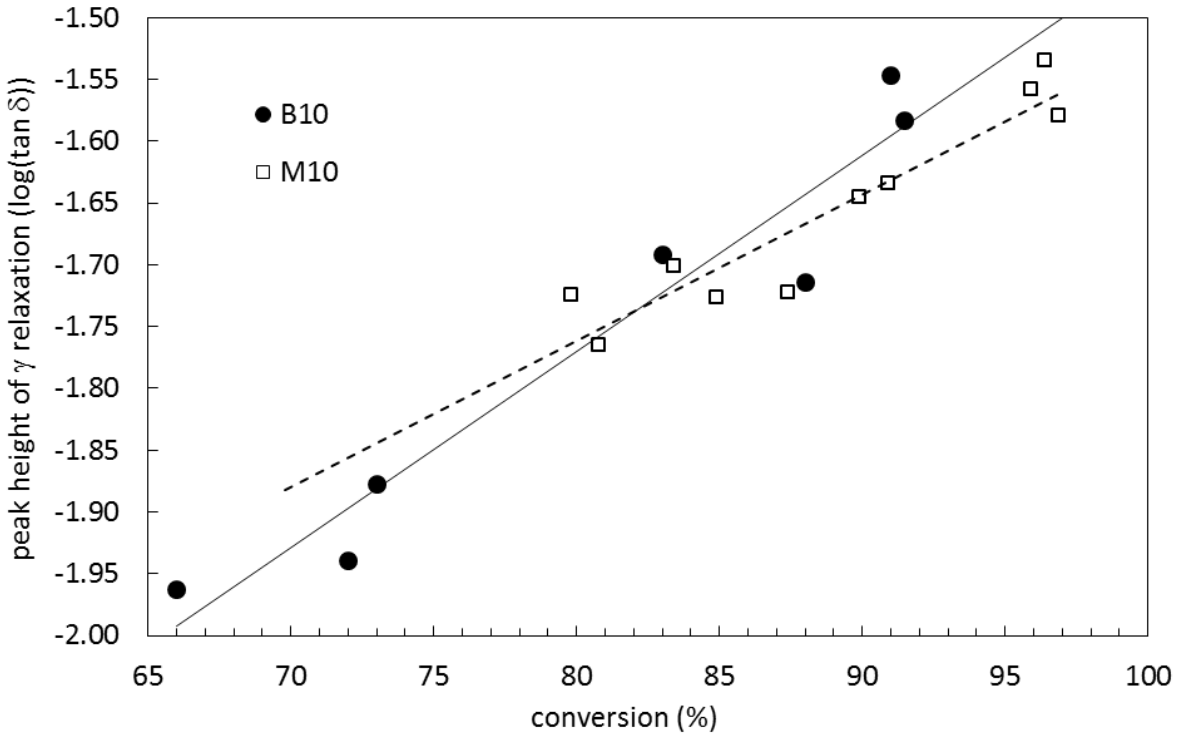


Fig. 8:

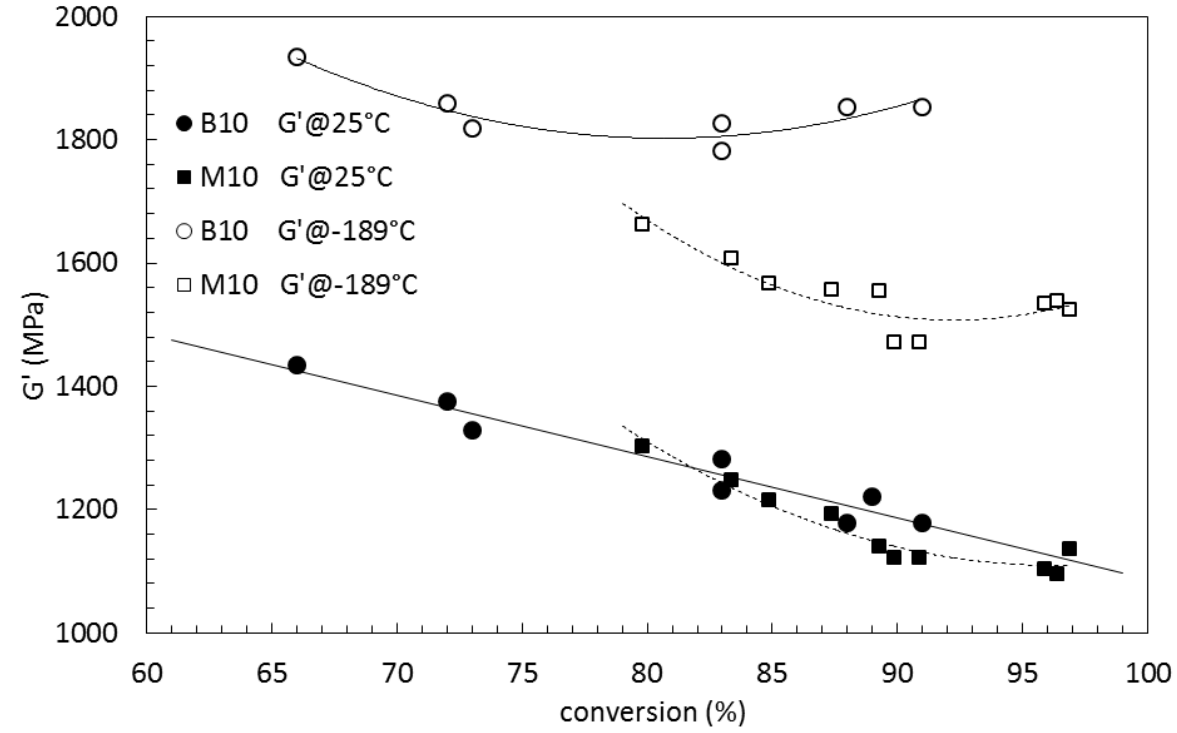


Fig. 9:

ACCEPTED MANUSCRIPT

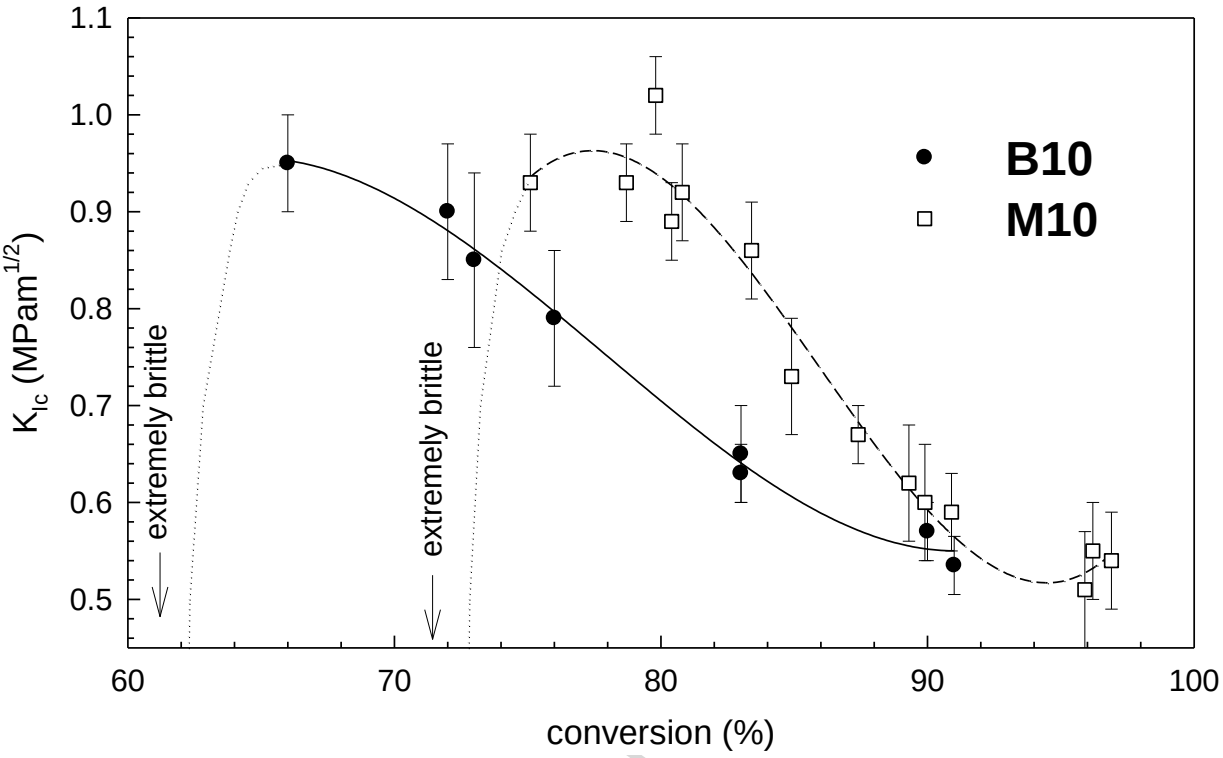


Fig. 10:

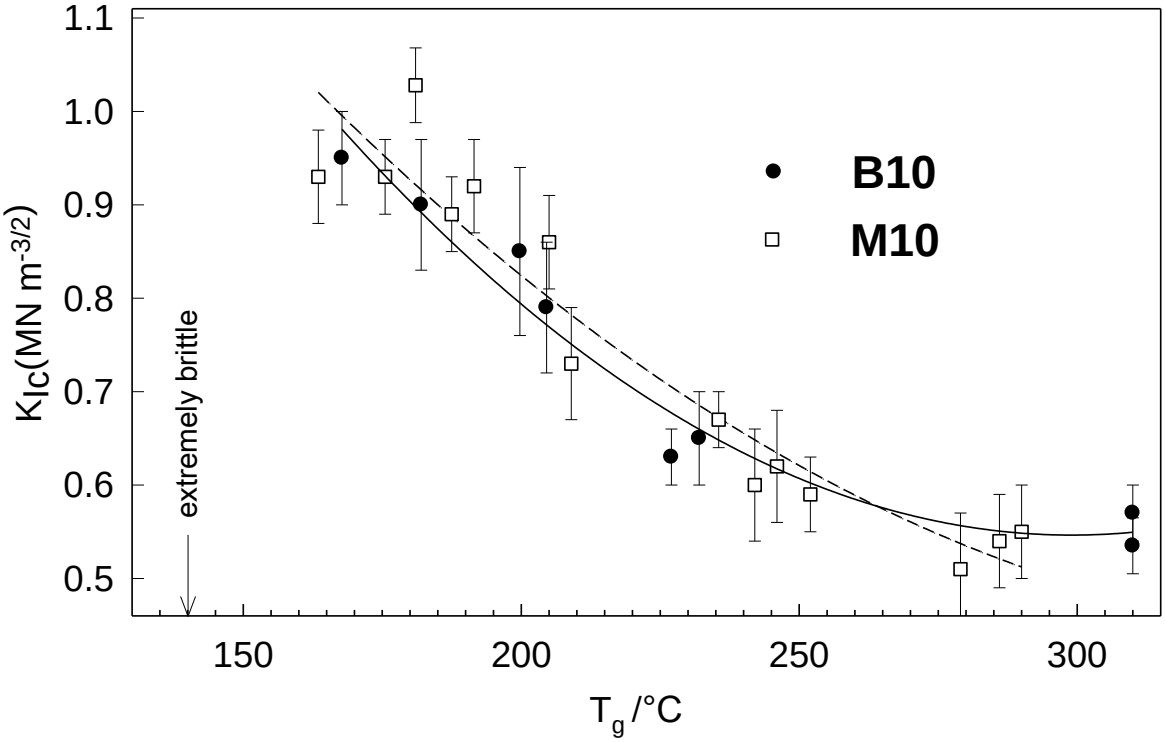


Fig. 11:

ACCEPTED MANUSCRIPT

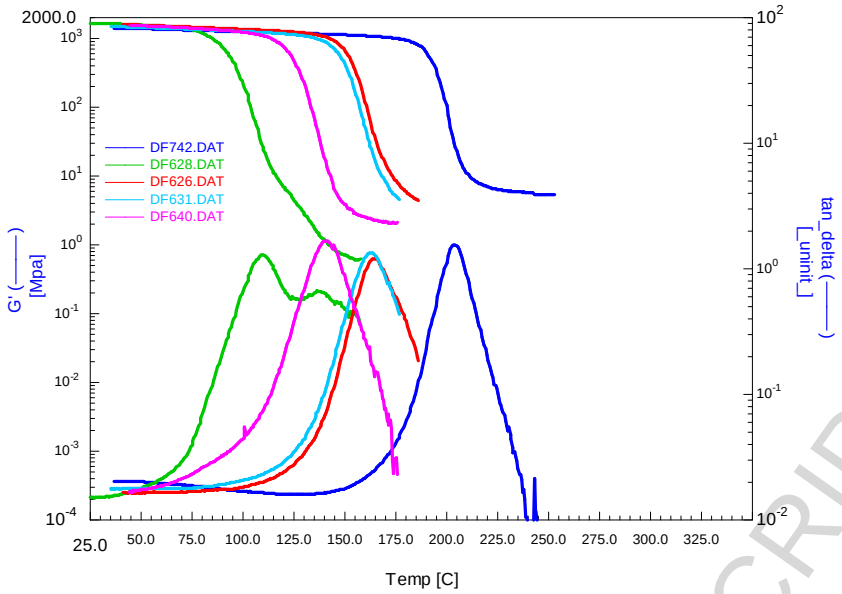


Fig. 12:

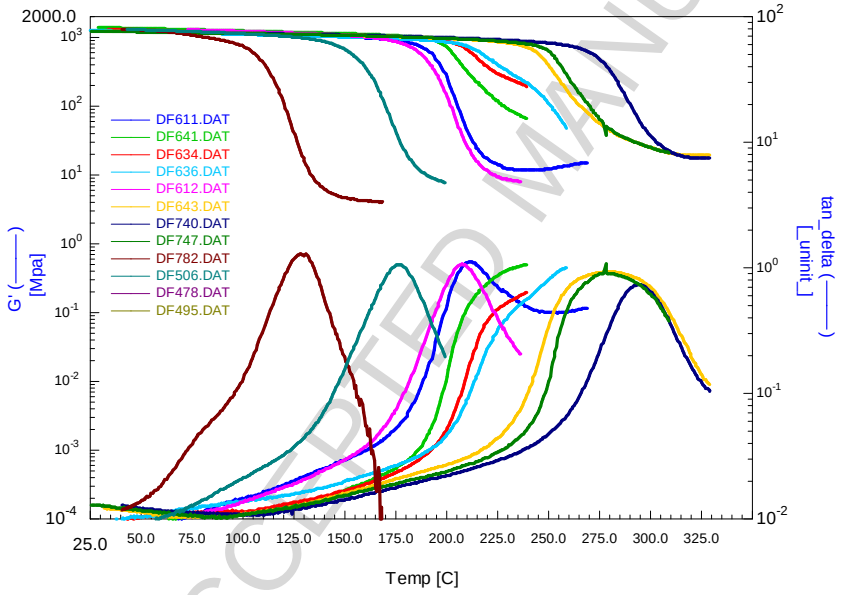


Fig. 13:

ACCEPTED MANUSCRIPT

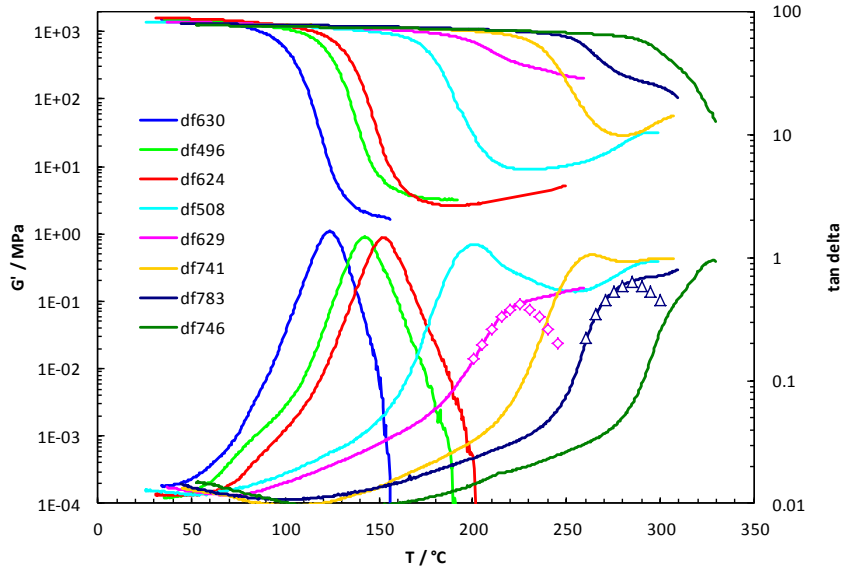


Fig. 14:

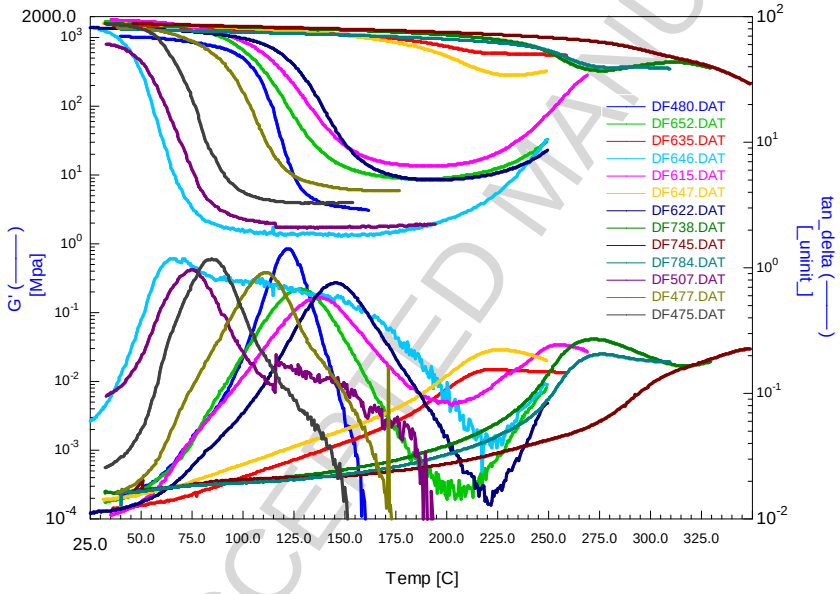


Fig. 15:

ACCEPTED MANUSCRIPT

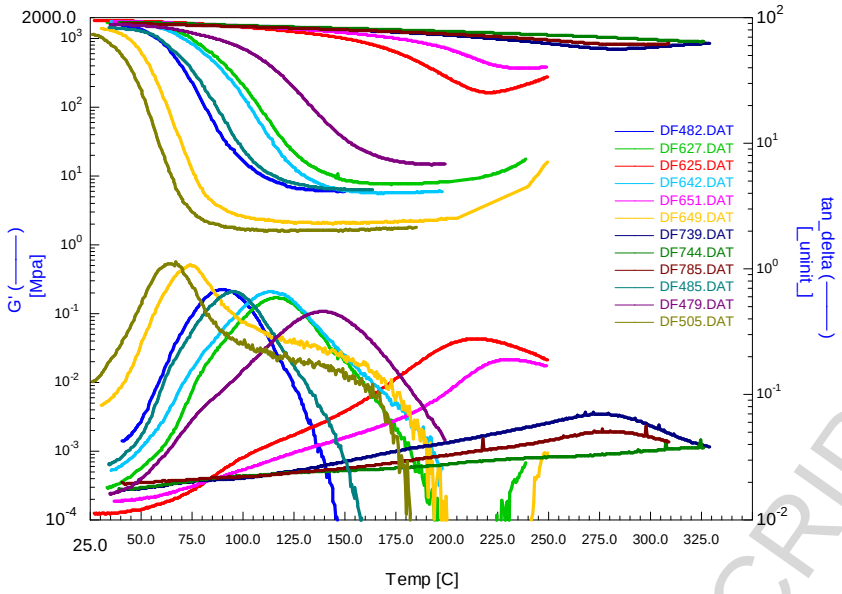


Fig. 16:

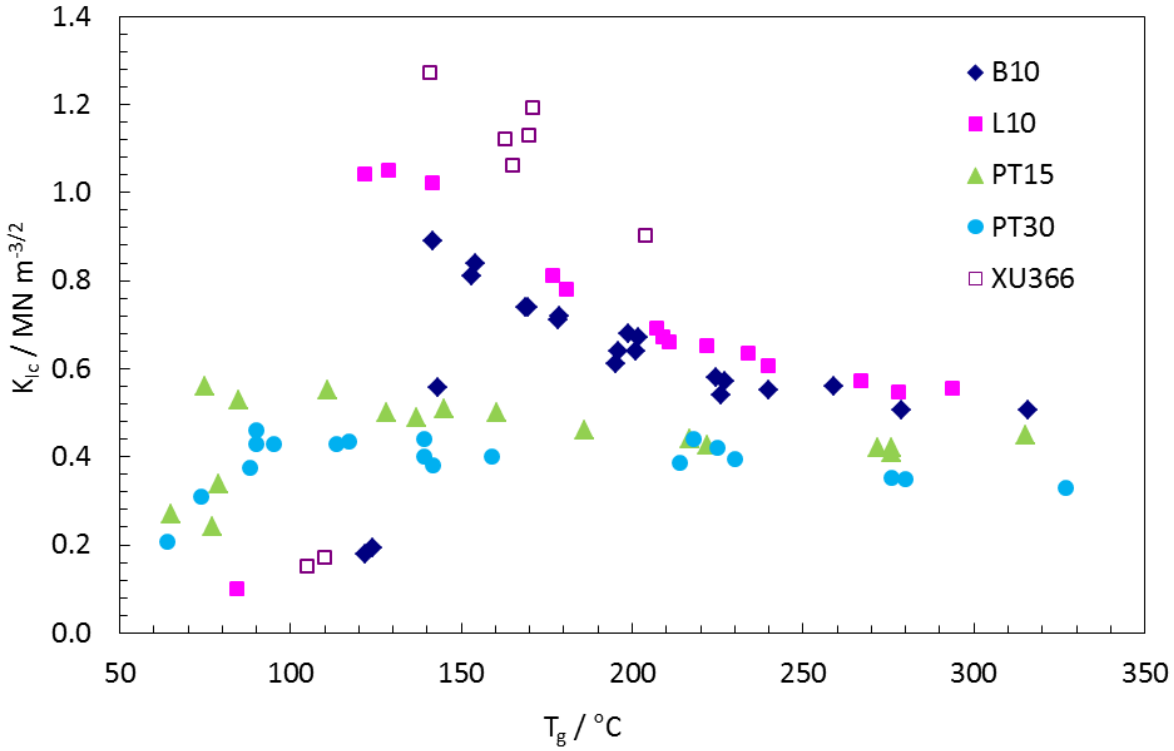


Fig. 17:

ACCEPTED MANUSCRIPT

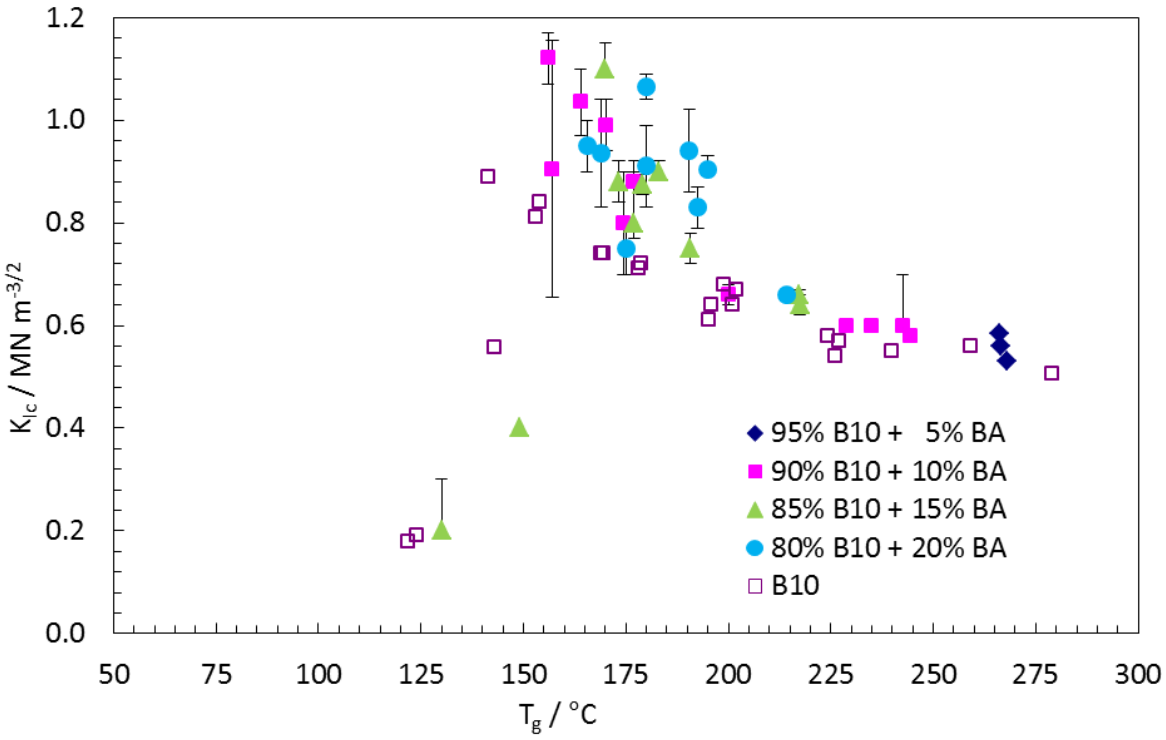


Fig. 18:

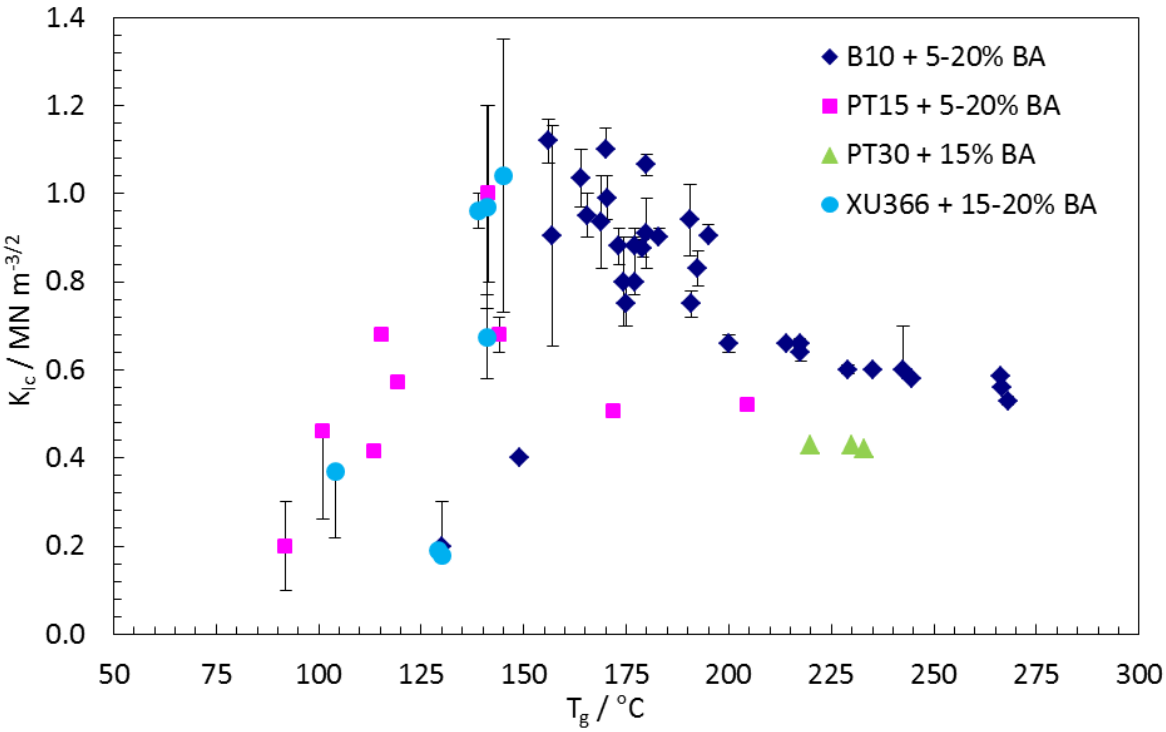


Fig. 19:

ACCEPTED MANUSCRIPT

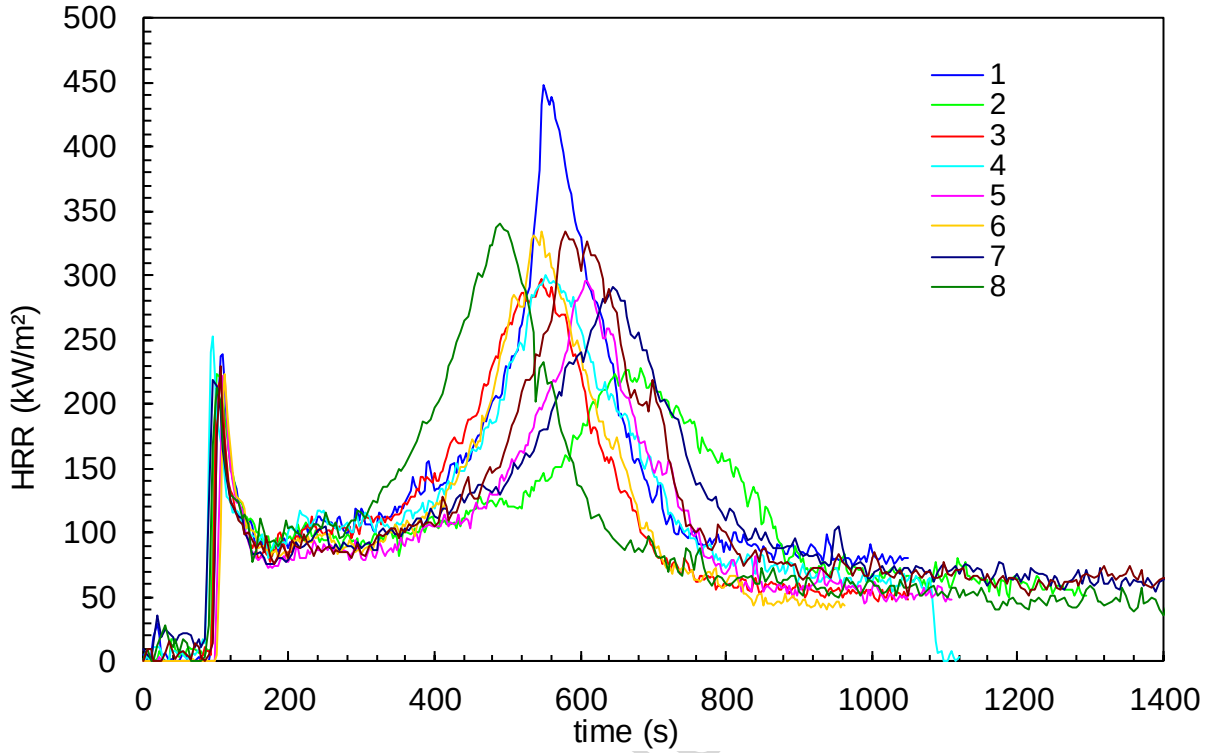


Fig. 20:

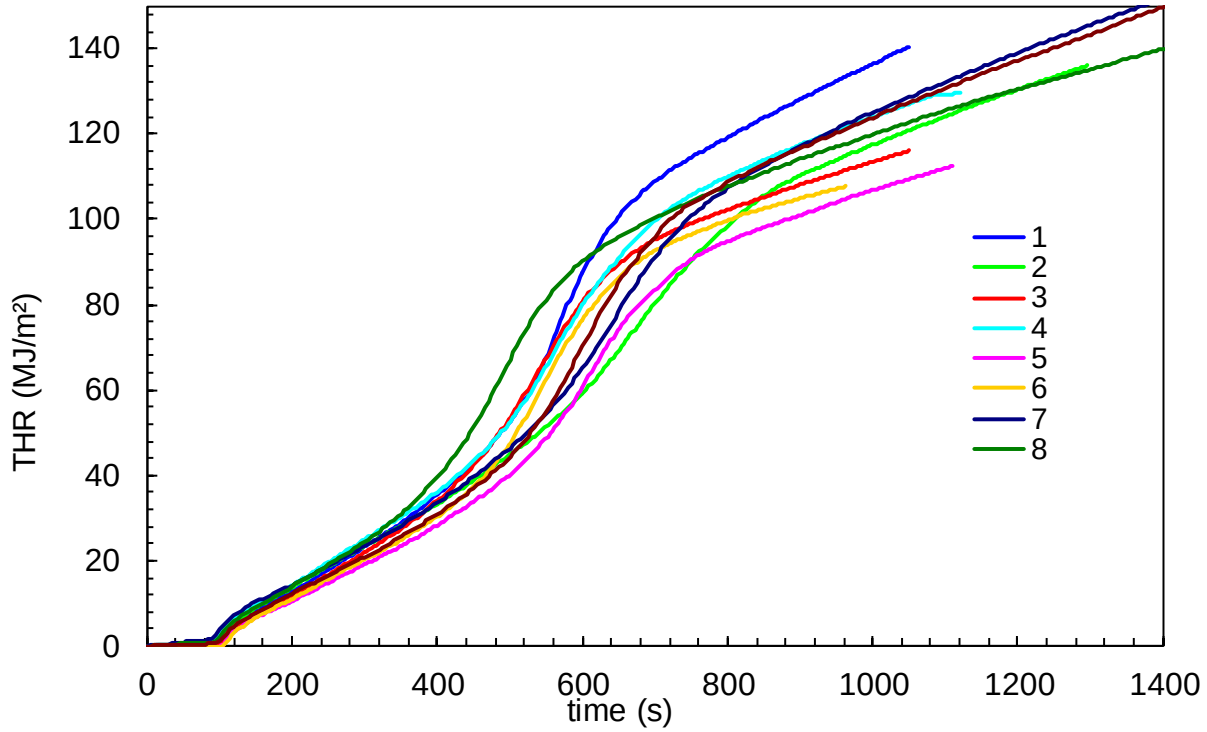


Fig. 21:

ACCEPTED MANUSCRIPT

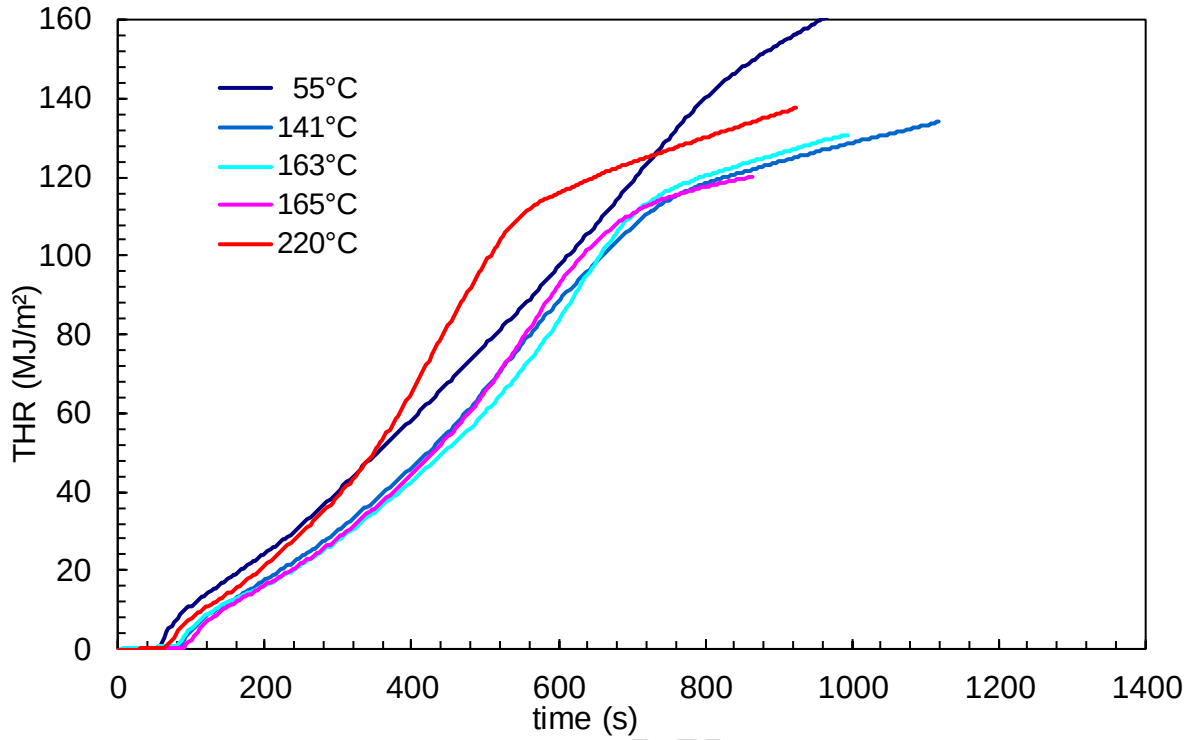


Fig. 22:

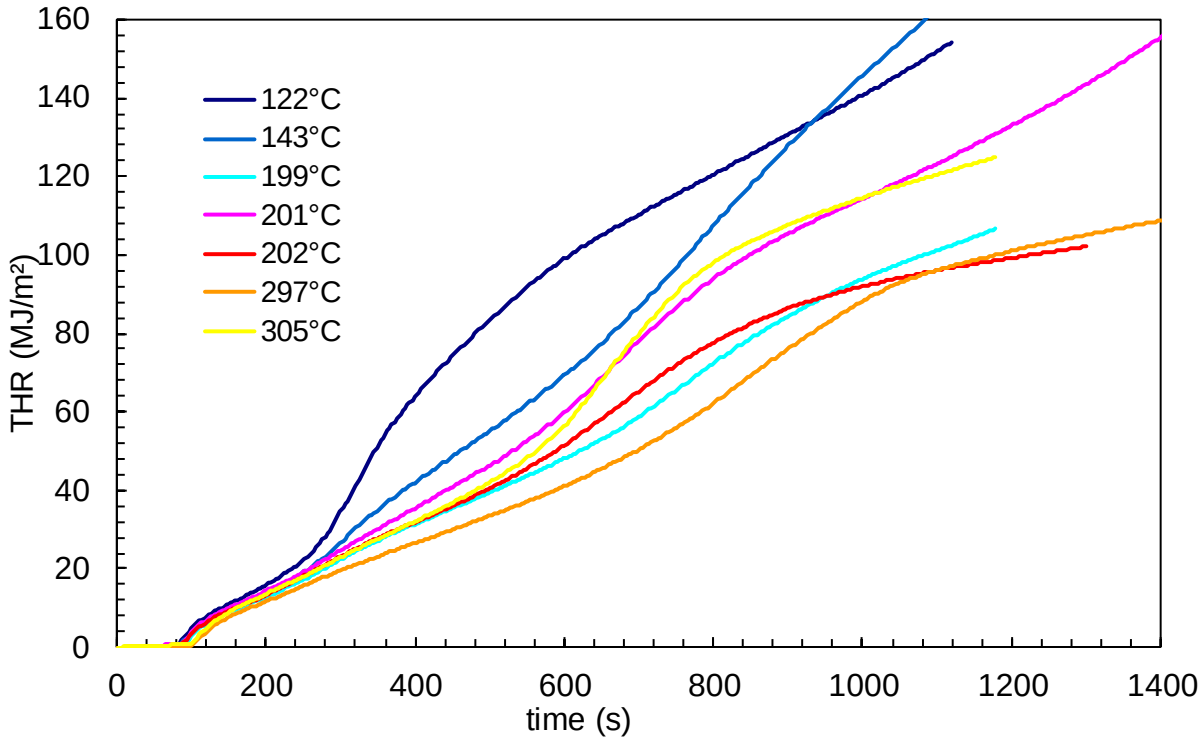


Fig. 23:

ACCEPTED MANUSCRIPT

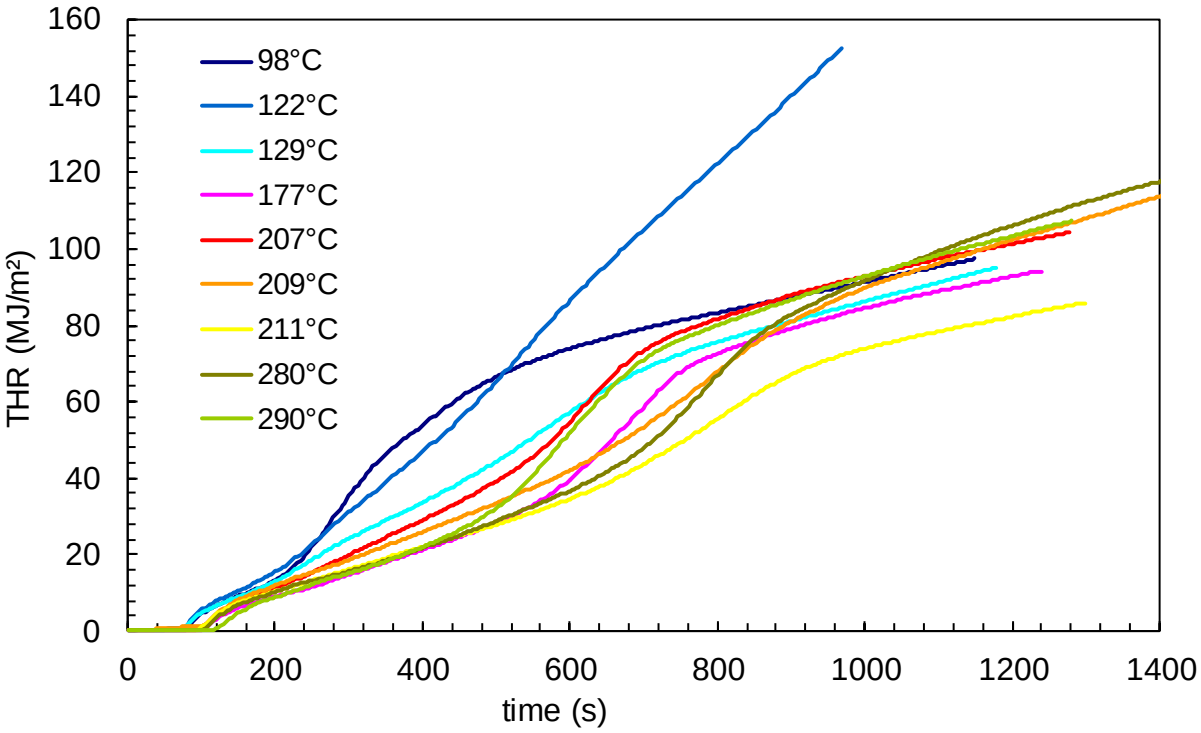


Fig. 24:

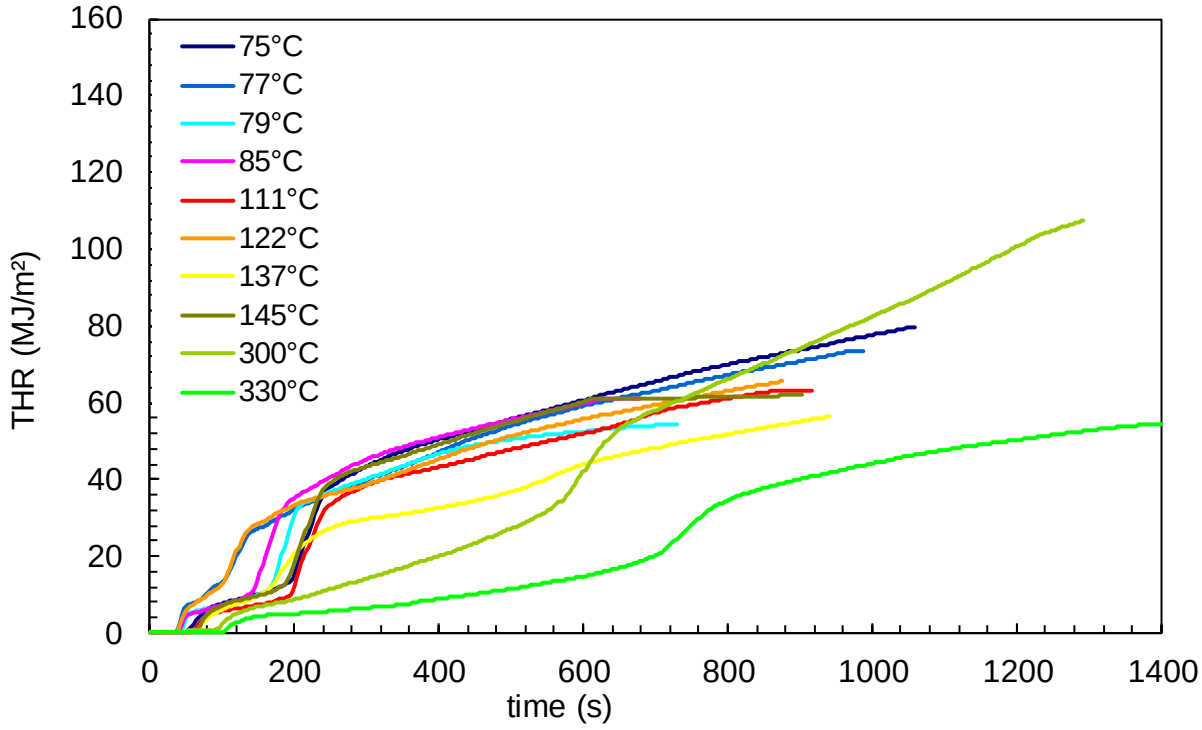


Fig. 25:

ACCEPTED MANUSCRIPT

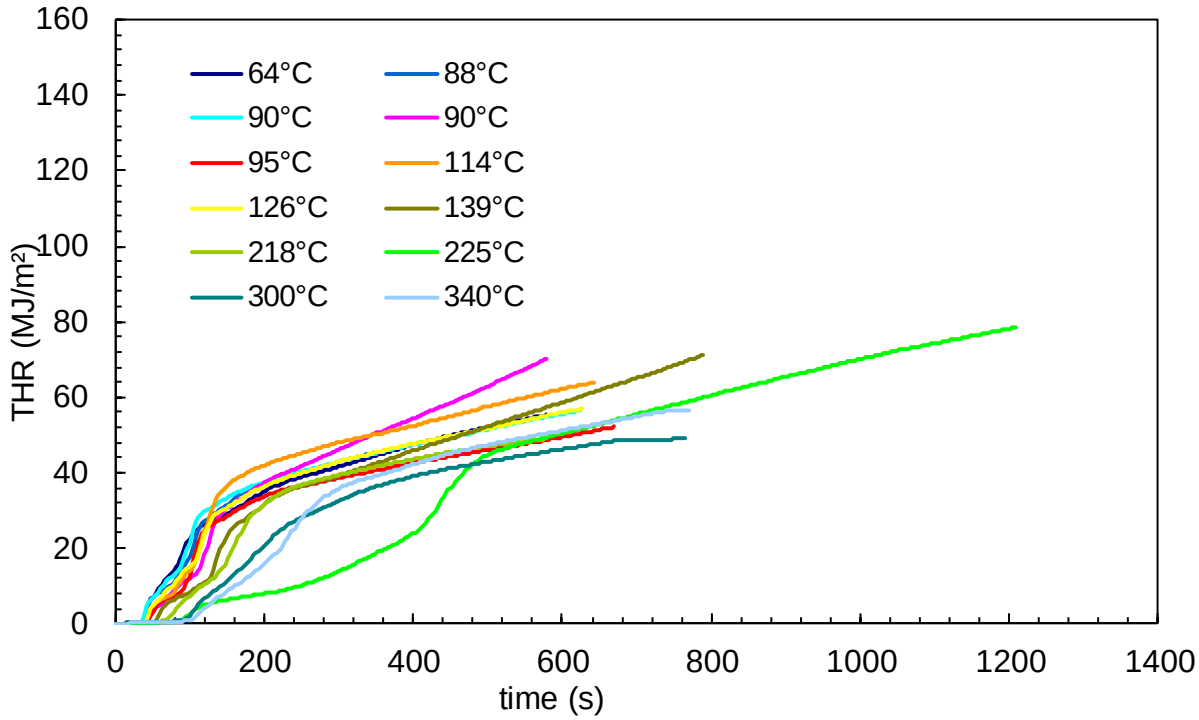


Fig. 26:

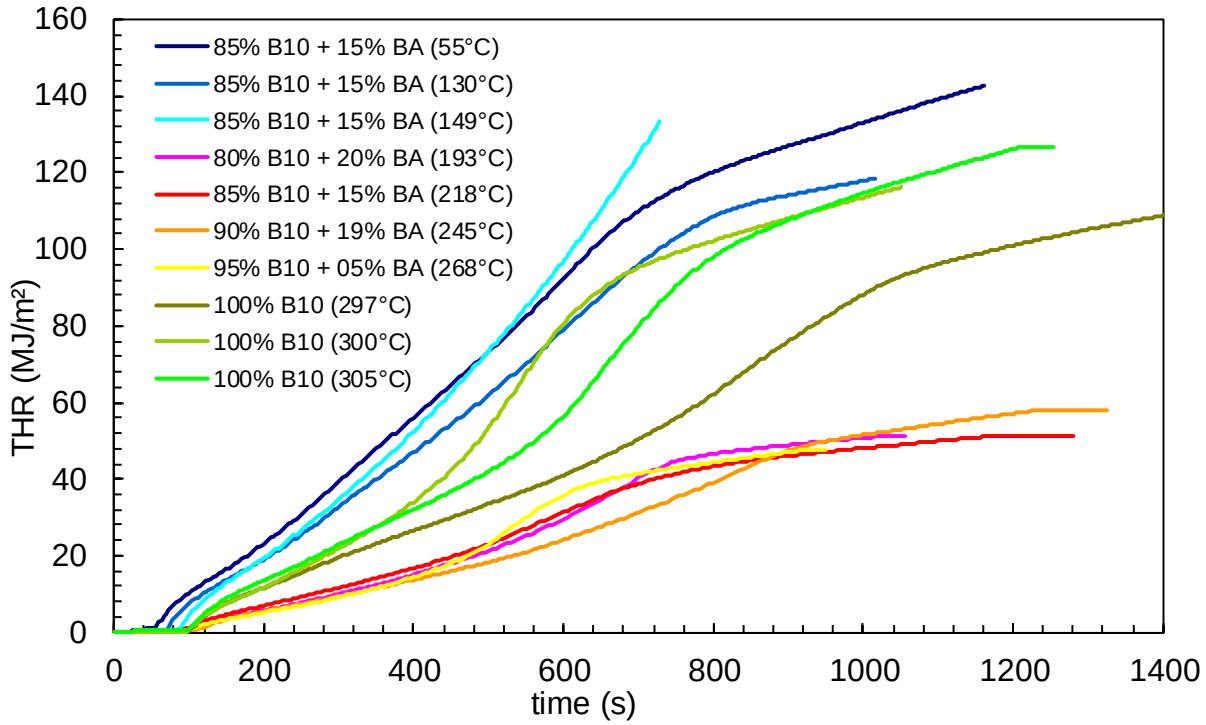


Fig. 27:

ACCEPTED MANUSCRIPT

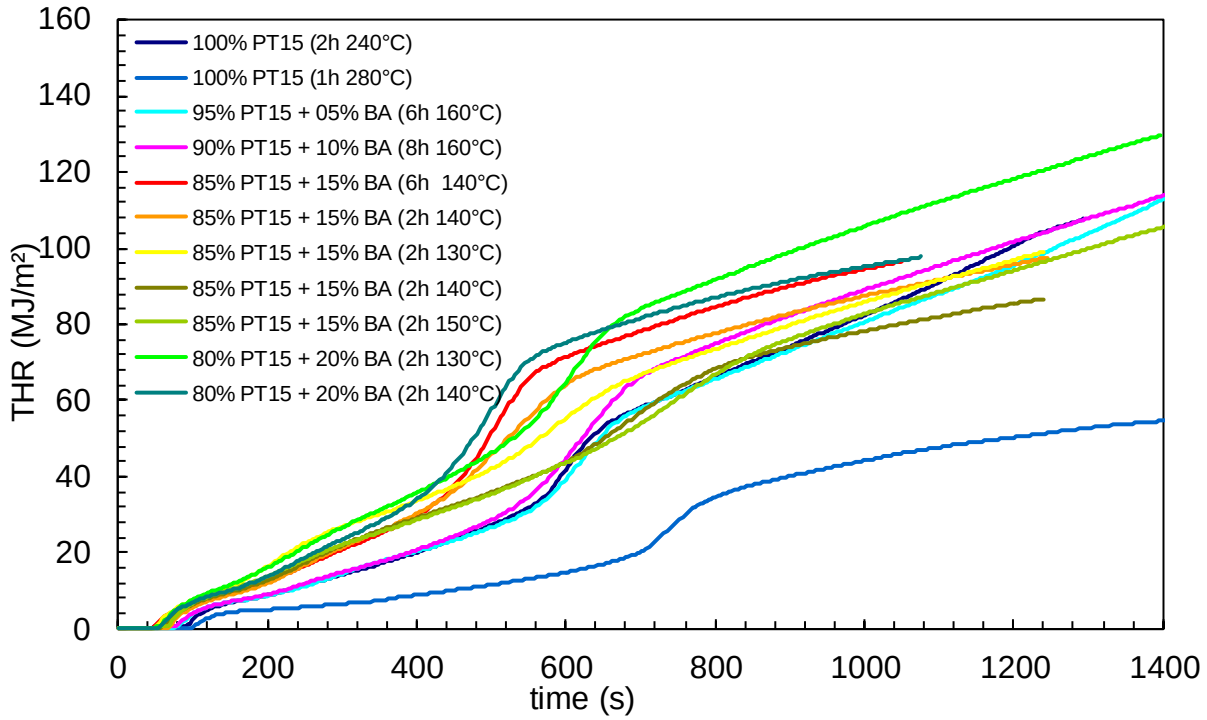


Fig. 28:

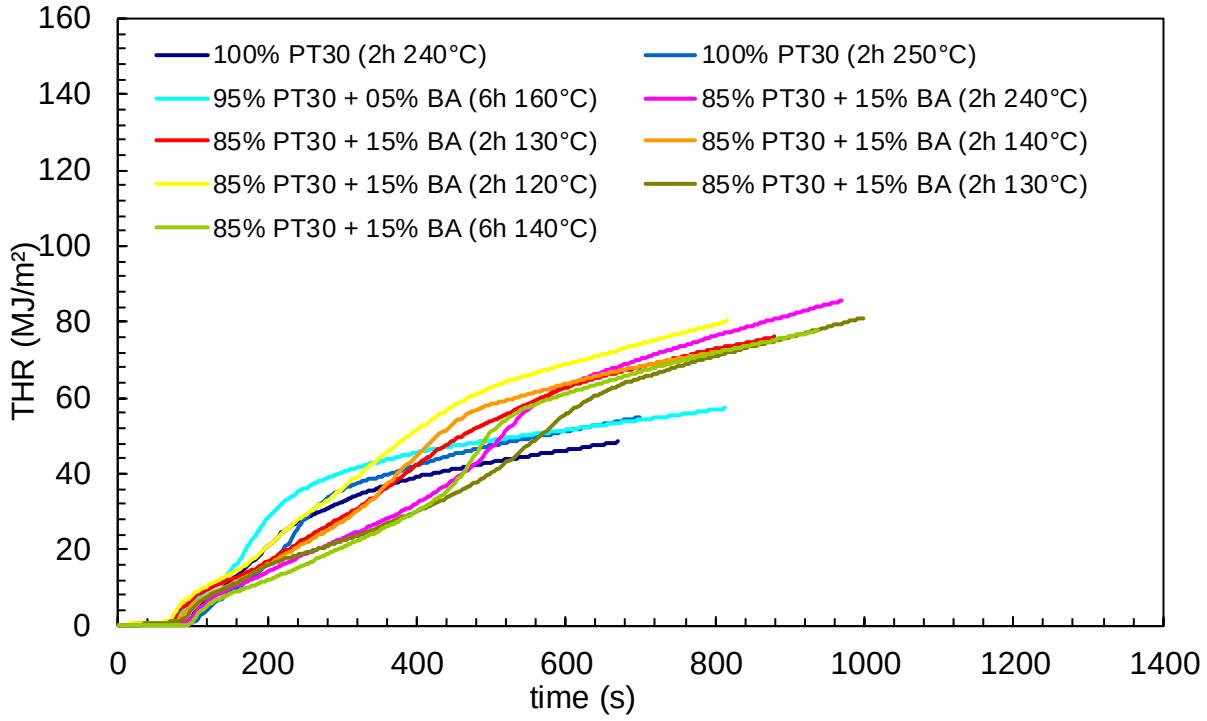


Fig. 29:

ACCEPTED MANUSCRIPT

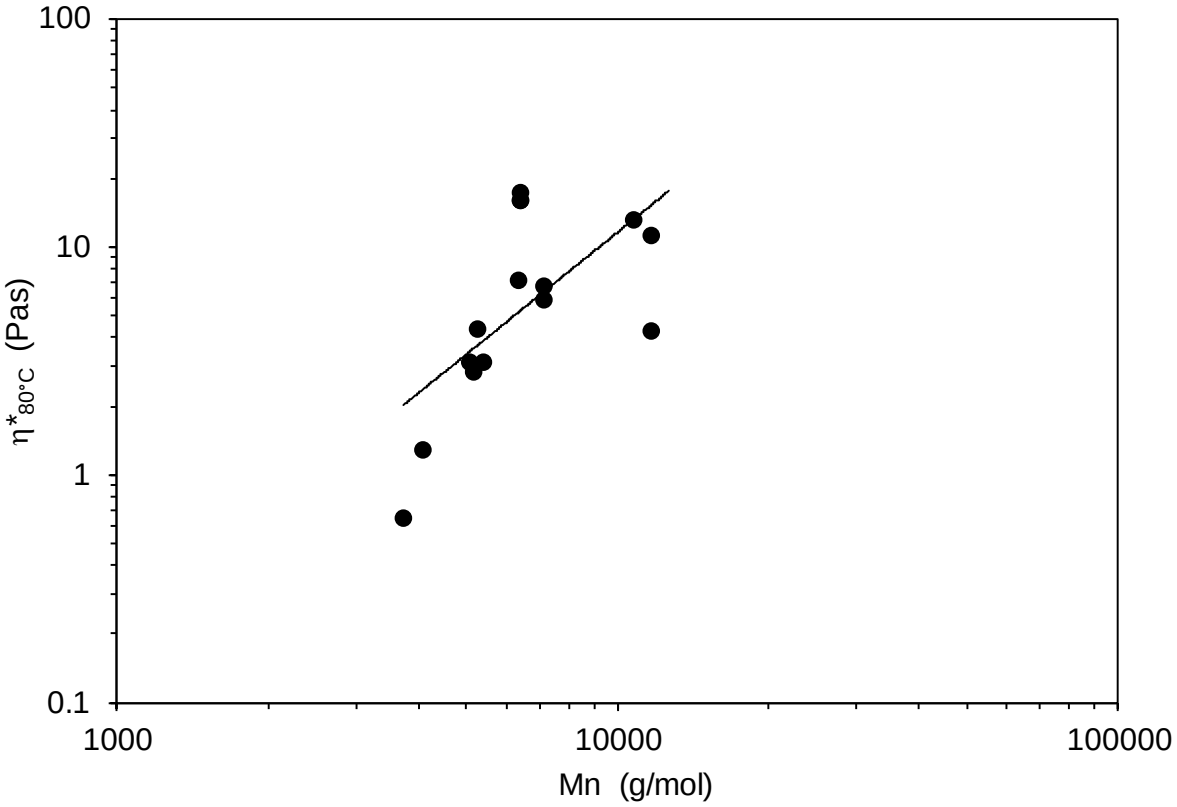


Fig. 30

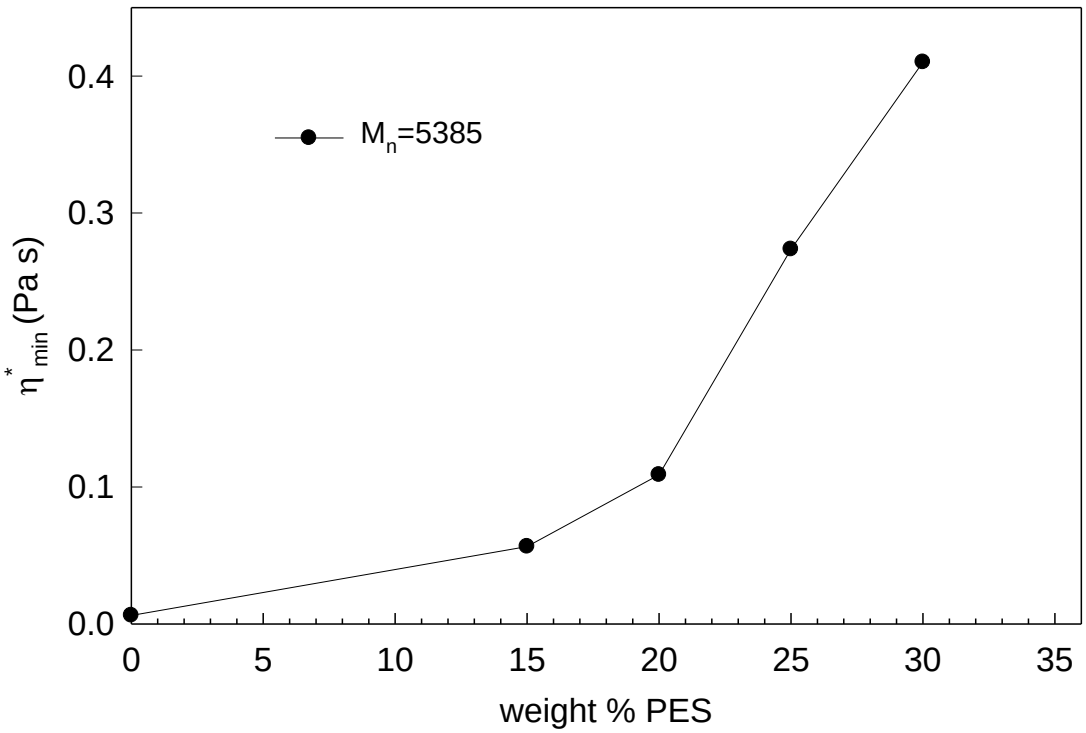


Fig. 31:

ACCEPTED MANUSCRIPT

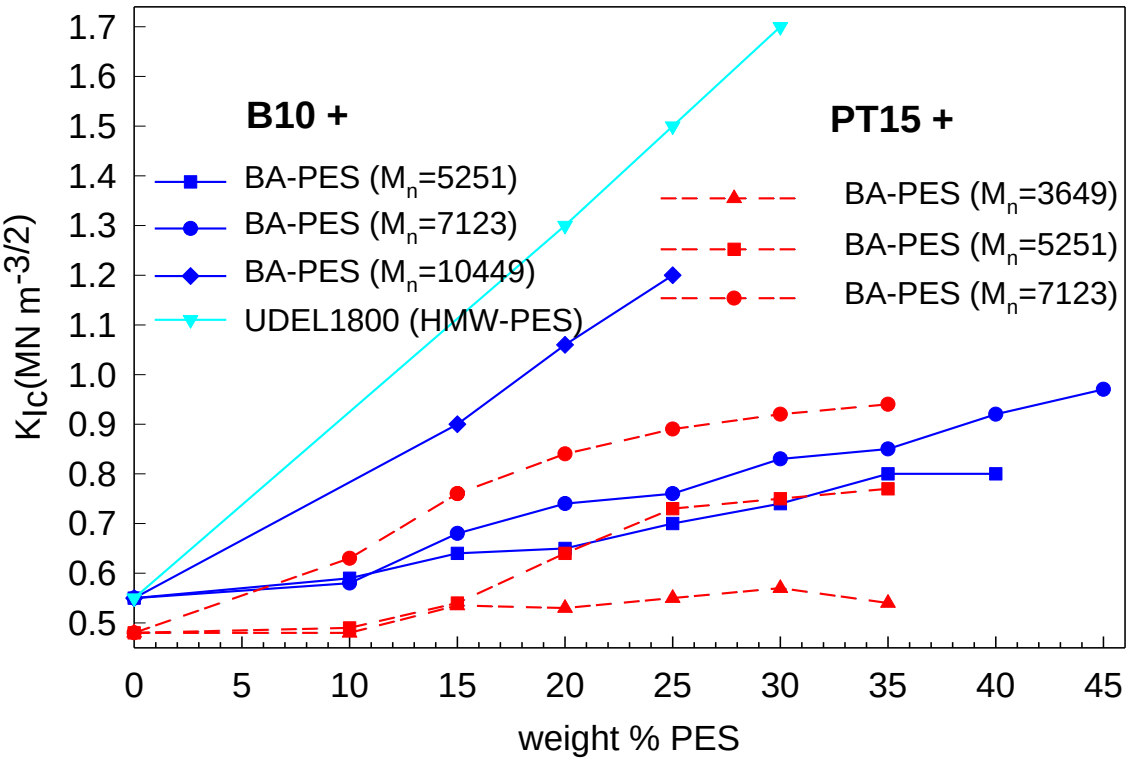


Fig. 32:

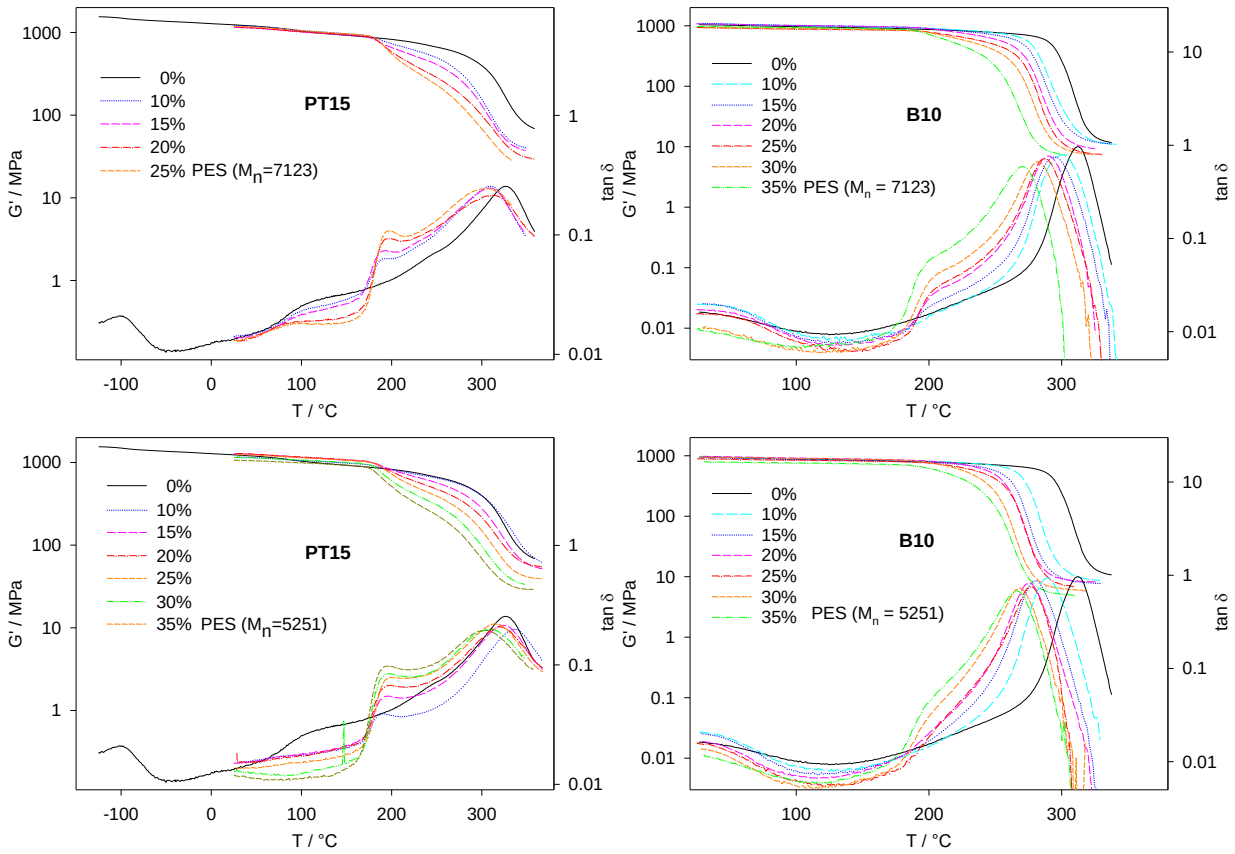


Fig. 33:

ACCEPTED MANUSCRIPT

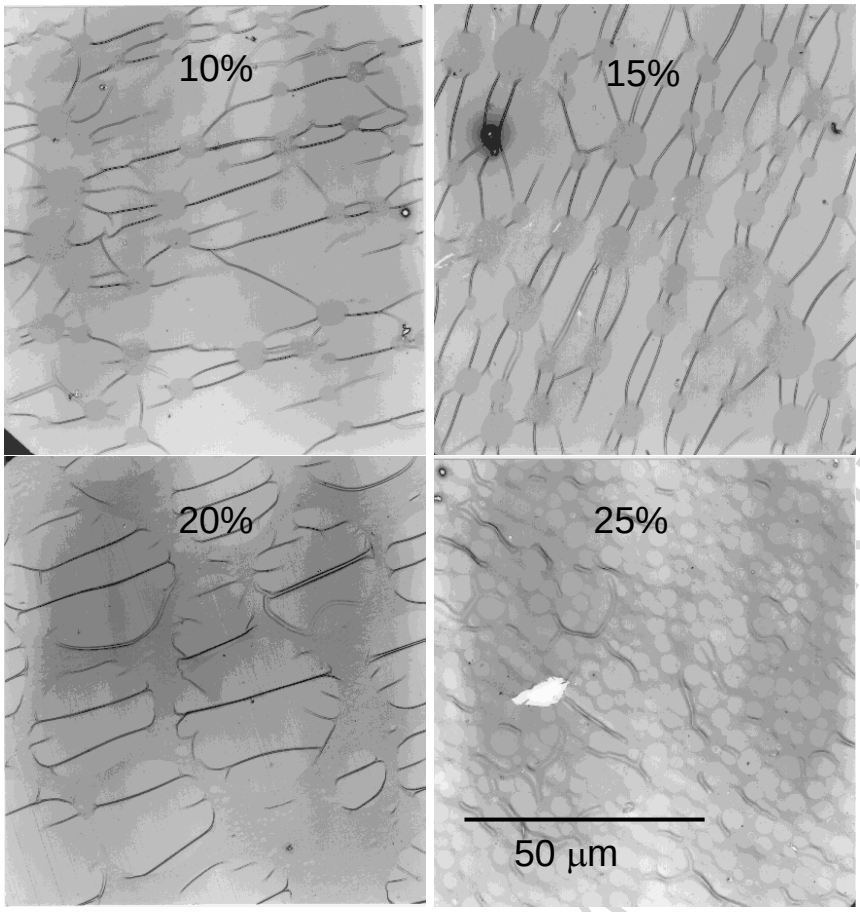


Fig. 34:

ACCEPTED MANUSCRIPT

ACCEPTED MANUSCRIPT

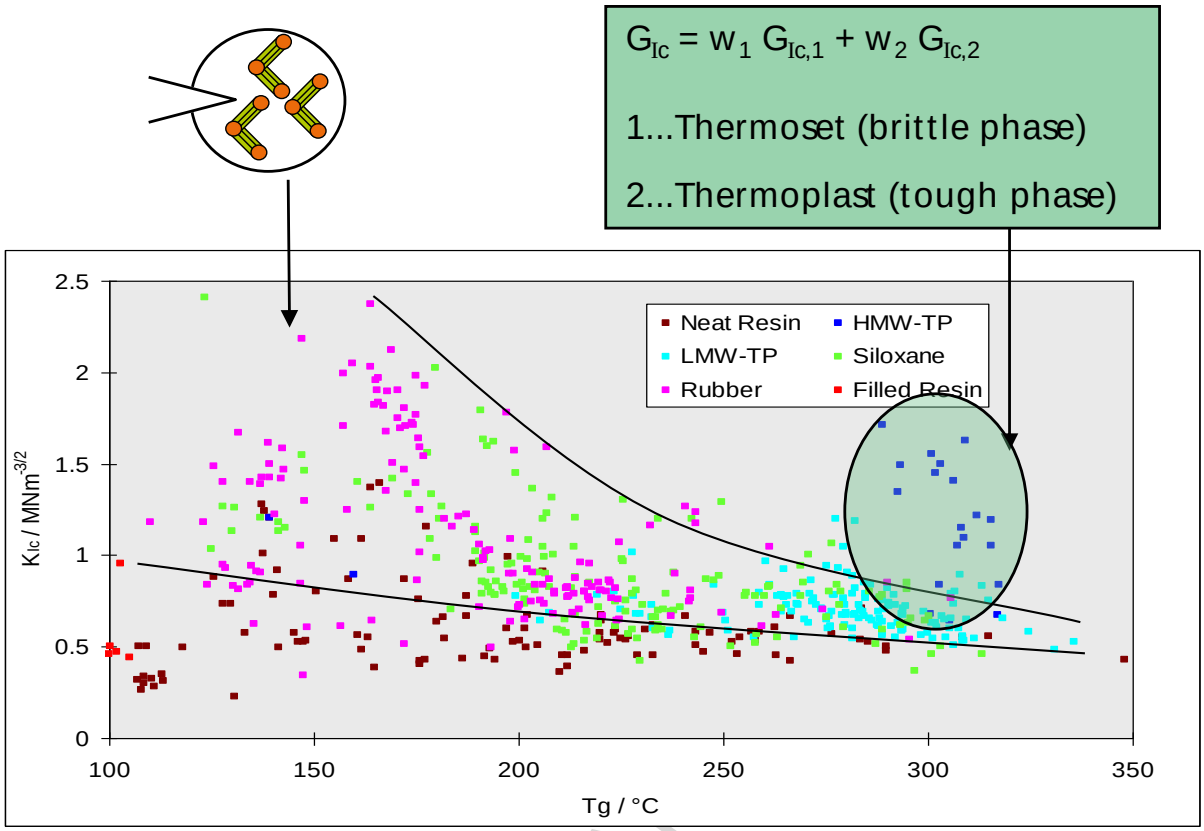


Fig. 35:

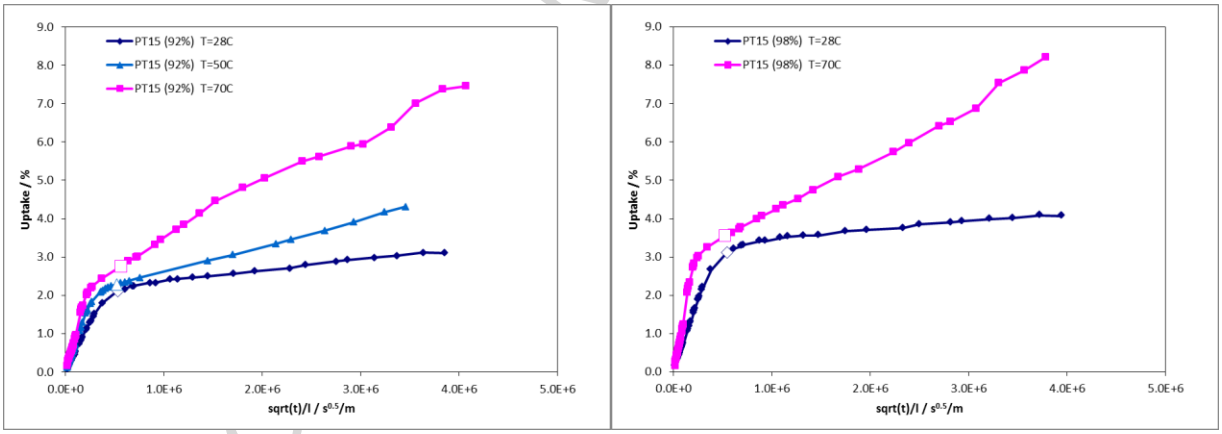


Fig. 36:

ACCEPTED MANUSCRIPT

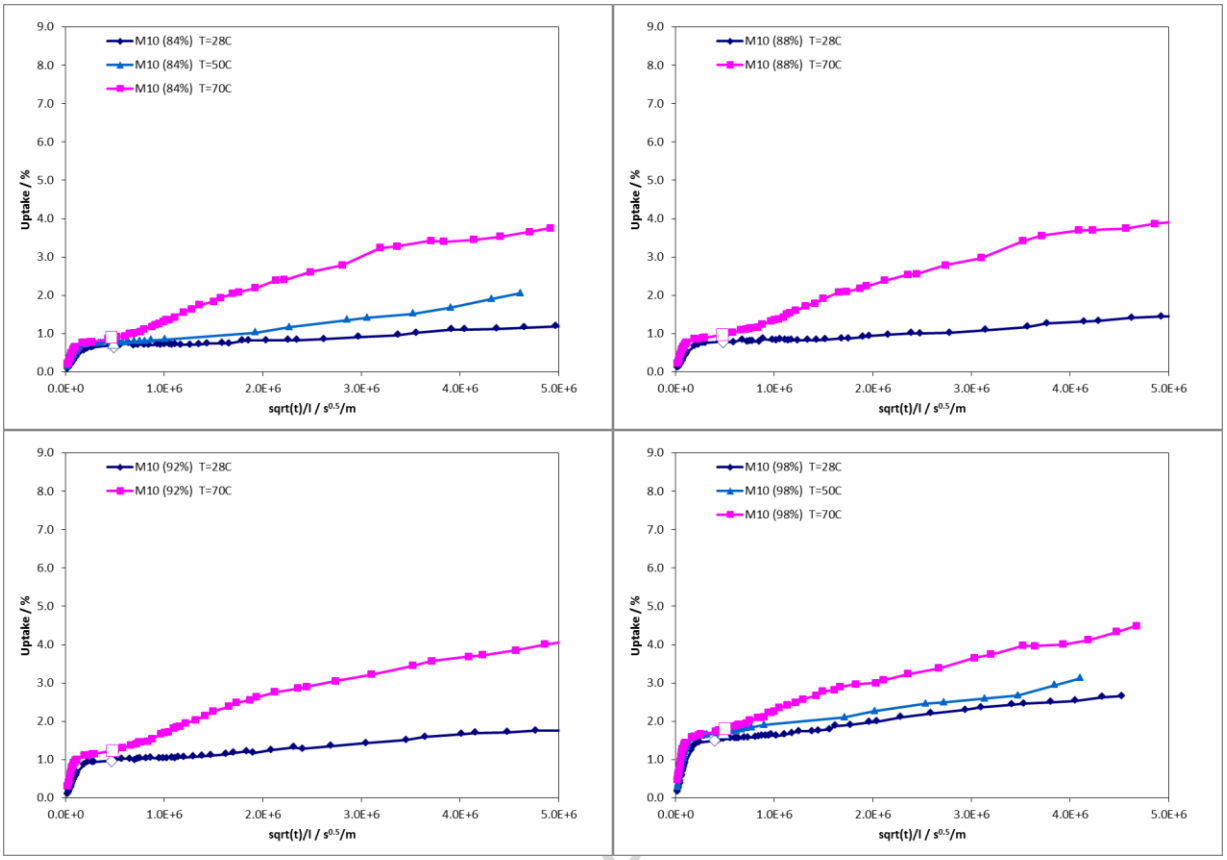


Fig. 37:

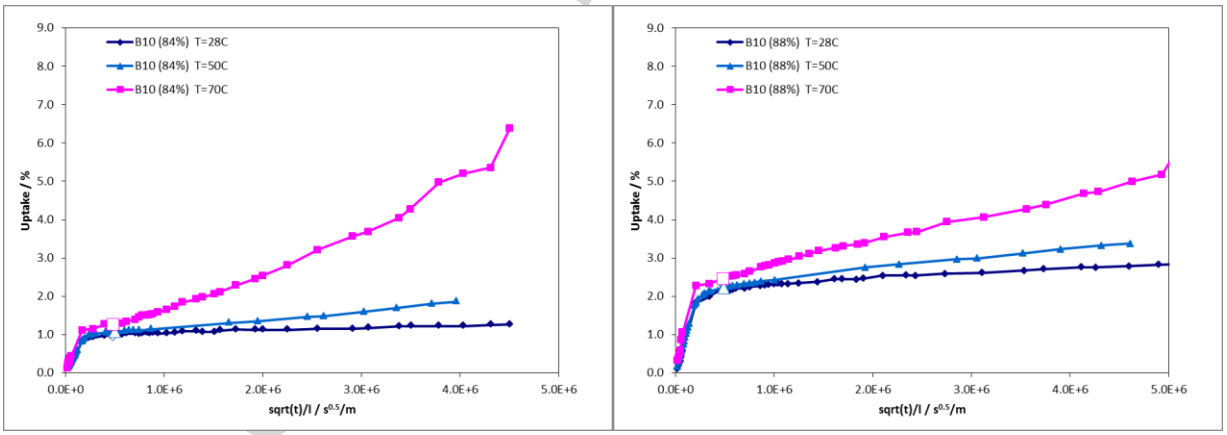


Fig. 38:

ACCEPTED MANUSCRIPT

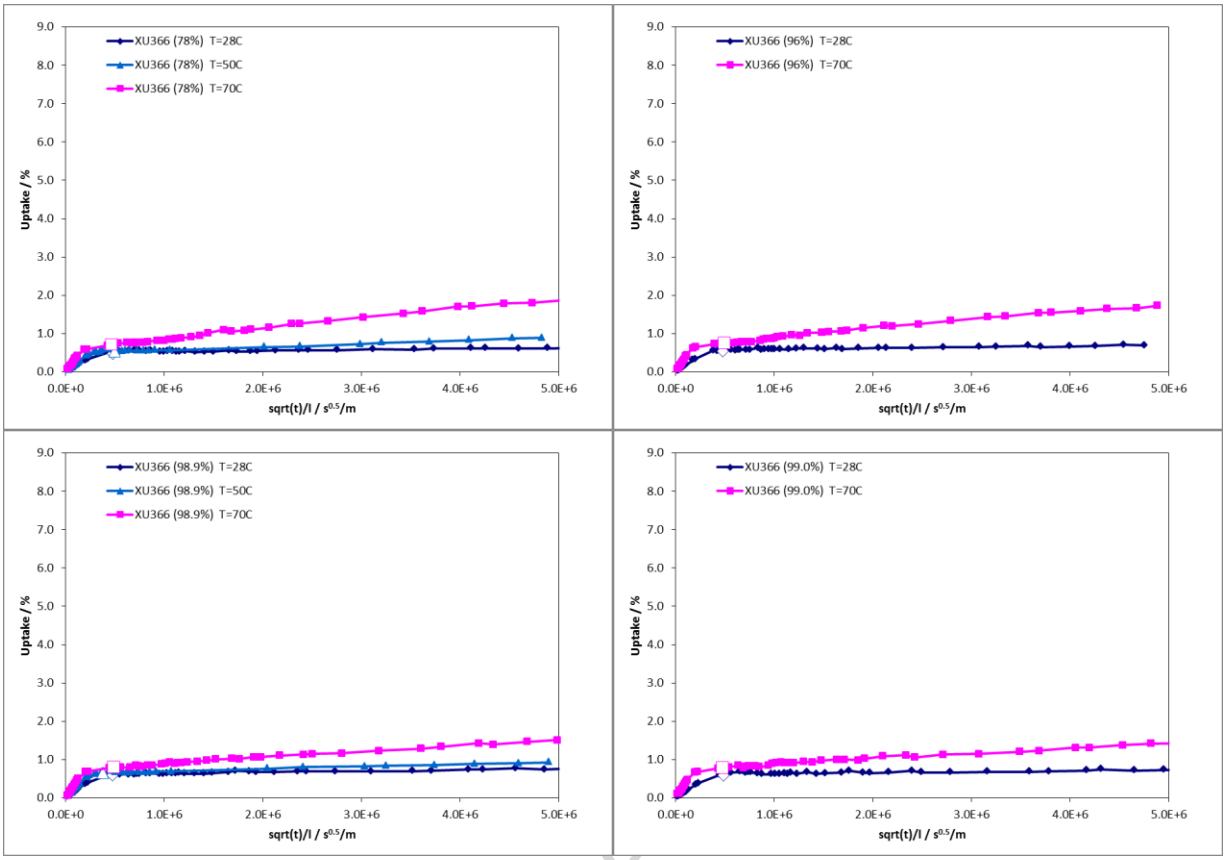


Fig. 39:

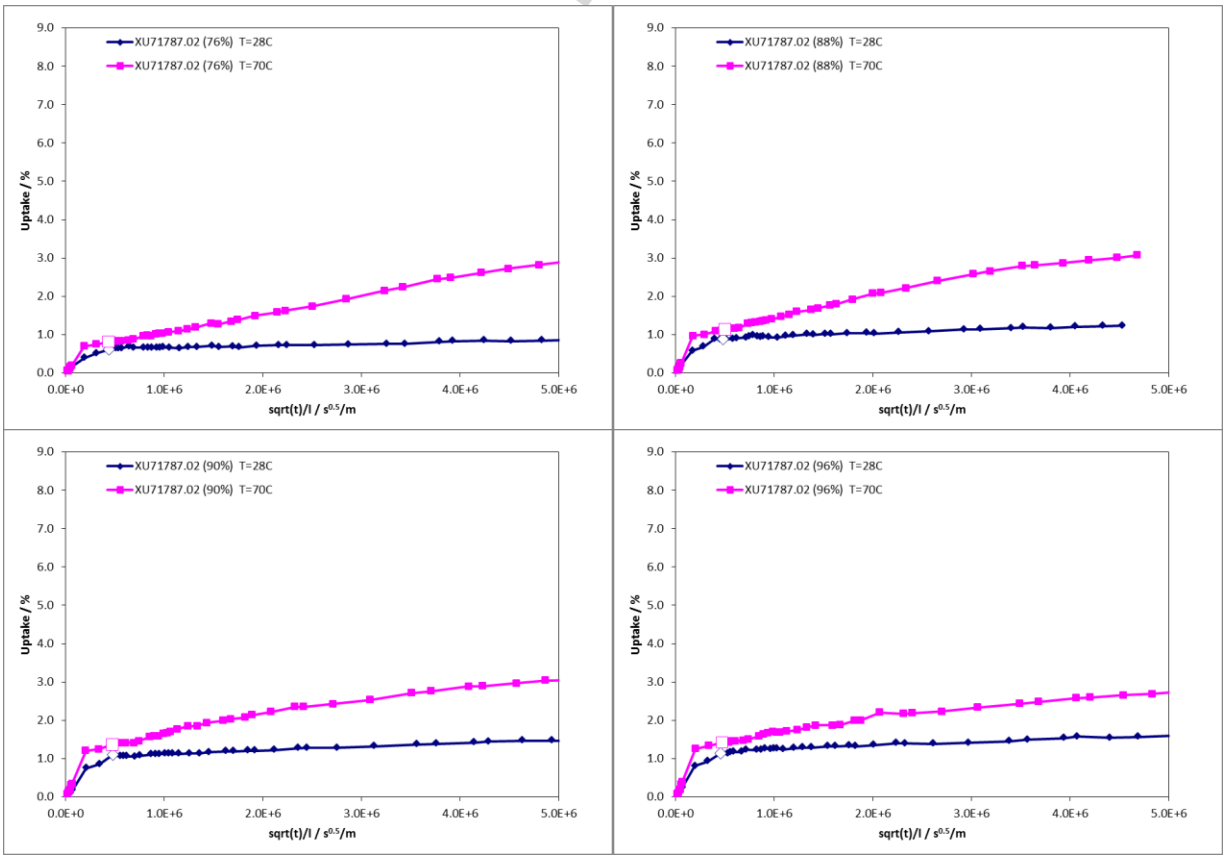


Fig. 40:

ACCEPTED MANUSCRIPT

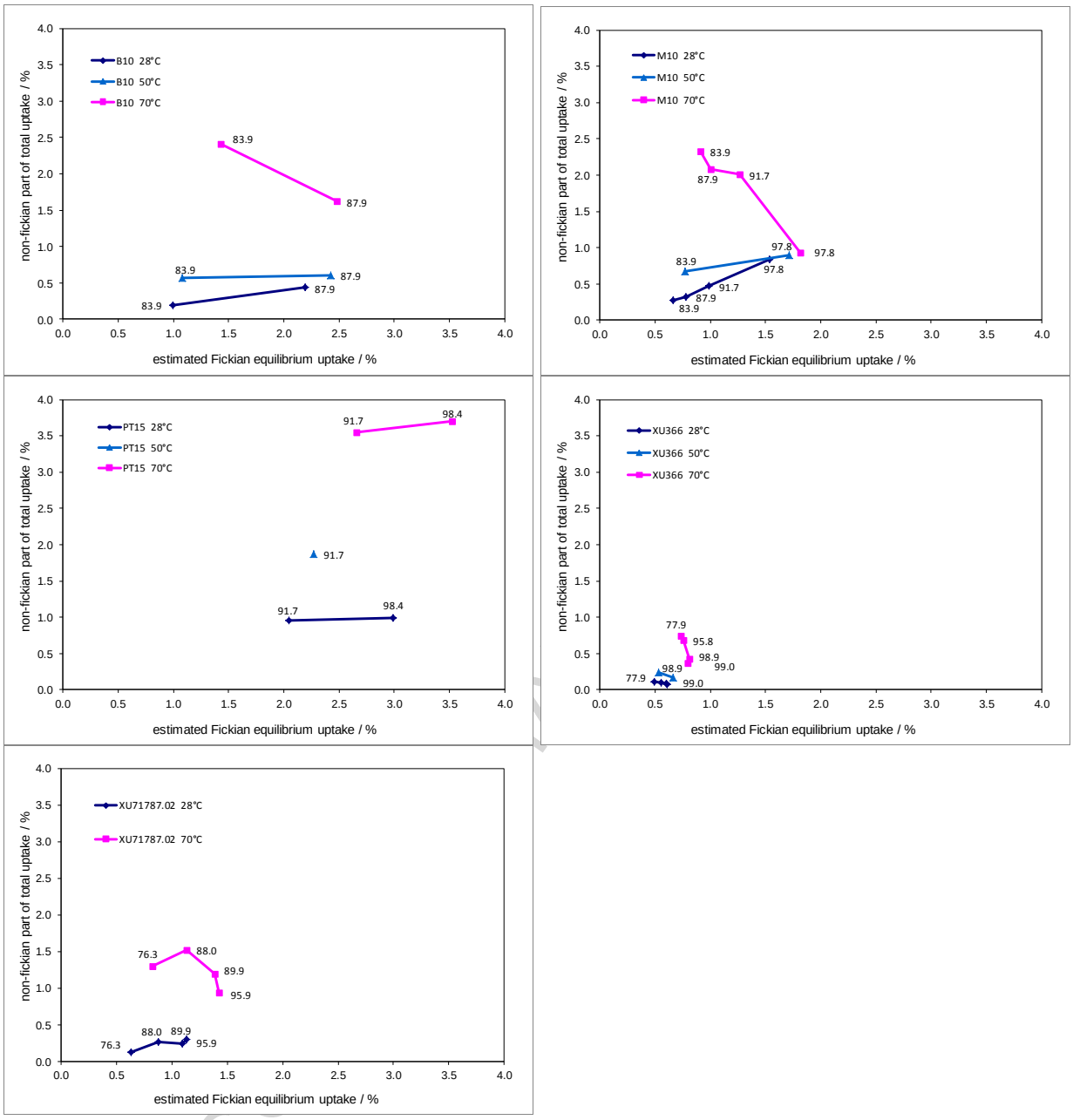


Fig. 41:

ACCEPTED MANUSCRIPT

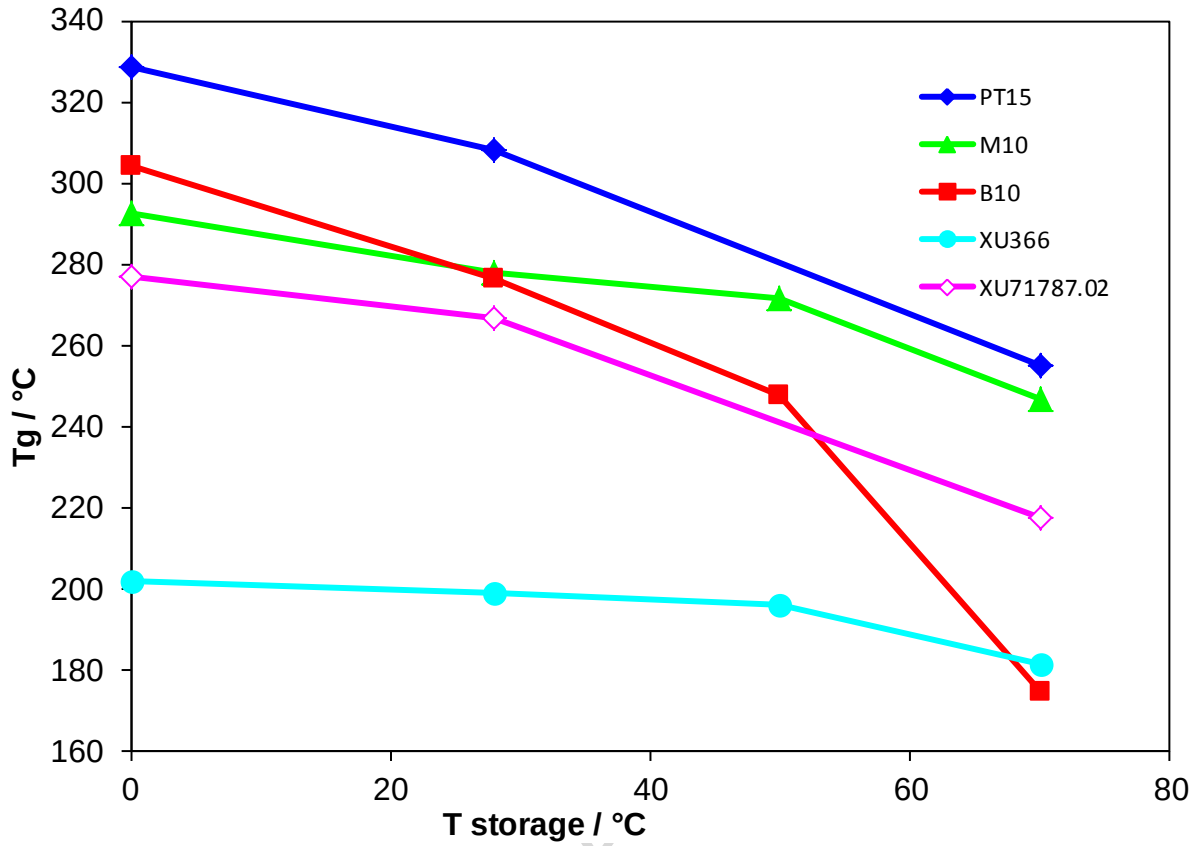


Fig. 42:

ACCEPTED MA

ACCEPTED MANUSCRIPT

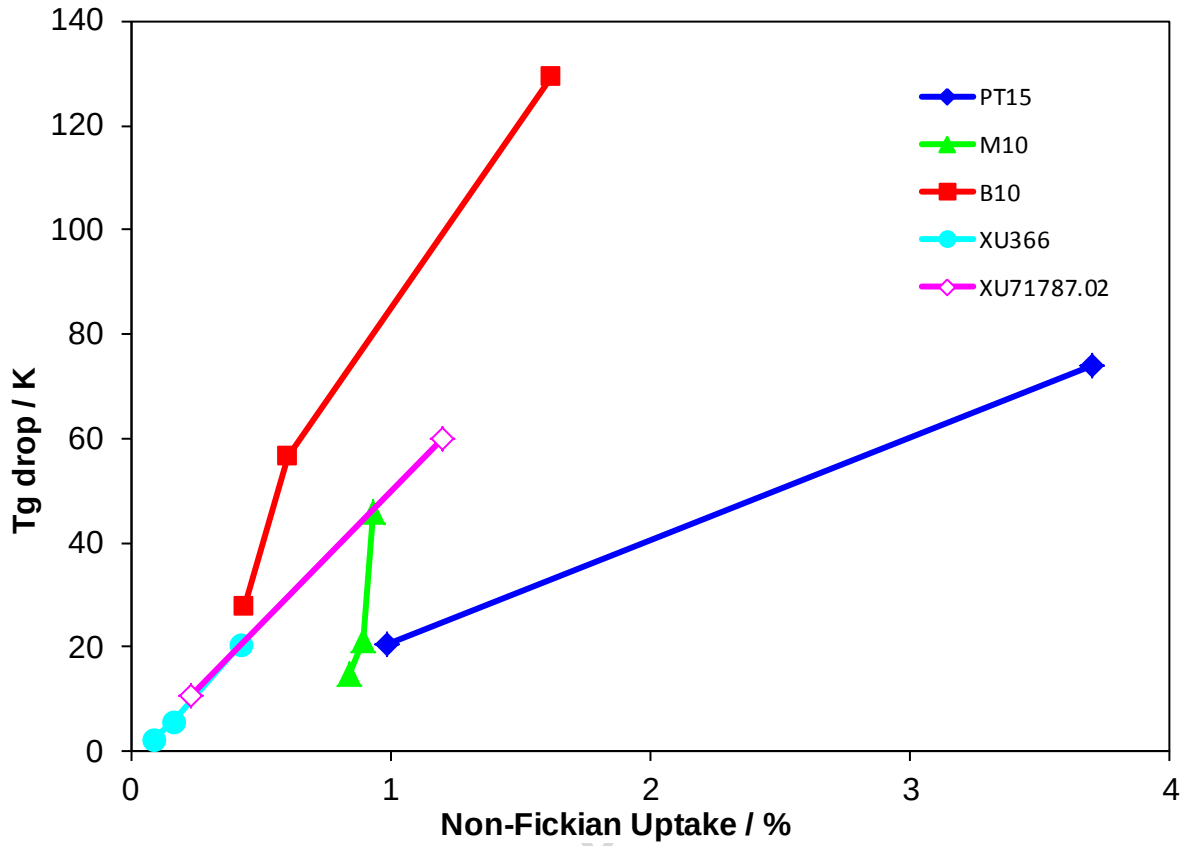


Fig. 43:

ACCEPTED MANUSCRIPT